University of Dundee

Data-Driven Classification of Spectral Profiles Reveals Brain Region-Specific Plasticity in Blindness

Lubinus, Christina; Orpella, Joan; Keitel, Anne; Gudi-Mindermann, Helene; Engel, Andreas K.; Roeder, Brigitte

Document Version
Peer reviewed version

[Link to publication in Discovery Research Portal](#)

1   **Data-Driven Classification of Spectral Profiles Reveals**

2   **Brain Region-Specific Plasticity in Blindness**

3   Christina Lubinus[1], Joan Orpella[2], Anne Keitel[3], Helene Gudi-Mindermann[4,5], Andreas K.
4   Engel[6], Brigitte Roeder[4], Johanna M. Rimmele[1,6,*]

5

6   <u>Running title:</u> Region-specific Spectral Plasticity

7
8
9   [1]Department of Neuroscience
10   Max-Planck-Institute for Empirical Aesthetics
11   Grüneburgweg 14
12   D - 60322 Frankfurt am Main, Germany

13
14   [2]Department of Psychology
15   New York University
16   6 Washington Place
17   New York, NY 10003, USA

18
19   [3] Psychology
20   University of Dundee
21   Scrymgeour Building
22   Dundee DD1 4HN, Scotland, UK

23
24   [4]Biological Psychology and Neuropsychology
25   University of Hamburg
26   Von-Melle-Park 11
27   20146 Hamburg, Germany

28
29   [5]Department of Social Epidemiology
30   University of Bremen
31   Grazer Straße 2
32   28359 Bremen, Germany

33
34   [6]Department of Neurophysiology and Pathophysiology
35   University Medical Center Hamburg-Eppendorf
36   Martinistraße 52
37   20246 Hamburg, Germany

38
39
40
41   <u>Corresponding author:</u>
42   Johanna M. Rimmele, PhD
43   Department of Neuroscience
44   Max-Planck-Institute for Empirical Aesthetics
45   Grüneburgweg 14
46   D - 60322 Frankfurt am Main, Germany
47   phone: +49 (69) 8300479-323
48   Email: johanna.rimmele@ae.mpg.de

1 **Abstract**

2 Congenital blindness has been shown to result in behavioral adaptation and neuronal reorgani-

3 zation, but the underlying neuronal mechanisms are largely unknown. Brain rhythms are char-

4 acteristic for anatomically defined brain regions and provide a putative mechanistic link to cog-

5 nitive processes. In a novel approach, using magnetoencephalography resting state data of con-

6 genitally blind and sighted humans, deprivation-related changes in spectral profiles were

7 mapped to the cortex using clustering and classification procedures. Altered spectral profiles in

8 visual areas suggest changes in visual alpha-gamma band inhibitory-excitatory circuits. Re-

9 markably, spectral profiles were also altered in auditory and right frontal areas showing in-

10 creased power in theta-to-beta frequency bands in blind compared to sighted individuals, pos-

11 sibly related to adaptive auditory and higher-cognitive processing. Moreover, occipital alpha

12 correlated with microstructural white matter properties extending bilaterally across posterior

13 parts of the brain. We provide evidence that visual deprivation selectively modulates spectral

14 profiles, possibly reflecting structural and functional adaptation.

15

16   *Keywords:* congenital blindness; MEG; oscillations; spectral fingerprints

17

18

1 Introduction

Brain rhythms occur ubiquitously across cortex (Buzsáki 2004; Buzsáki et al. 2013; Singer 2018) and have been related to cognitive functions. Investigating changes in brain rhythms in congenital blindness can provide crucial insights into the neuronal mechanisms of behavioral changes as found in this population. Congenitally blind individuals perform better on various auditory, tactile, and higher-cognitive tasks compared to sighted controls (Bull et al. 1983; Lessard et al. 1998; Roeder et al. 2001; Amedi et al. 2003; Gougoux et al. 2005; Foecker et al. 2012), including tasks where certain aspects of temporal processing are essential, such as in temporal order processing tasks, task involving musical meter or ultra-fast speech processing (Hoetting et al. 2004; Roeder et al. 2004; Stevens and Weaver 2005; Moos and Trouvain 2007; Roeder et al. 2007; Trouvain 2007; Hertrich et al. 2009; Dietrich et al. 2013; Lerens et al. 2014; Carrara-Augustenborg and Schultz 2019; Zhang et al. 2019). Improved behavioral performance in auditory or tactile tasks in congenitally blind individuals is accompanied by cross-modal plasticity. That is, the "visual" cortex has been observed to be recruited during non-visual tasks (Burton 2003; Pascual-Leone et al. 2005; Bedny et al. 2011; Voss and Zatorre 2012; Gudi-Mindermann et al. 2018; Rimmele et al. 2019), which has been postulated to functionally contribute to compensatory task performance. Additionally, intramodal plasticity has been observed in congenitally blind individuals. That is, the auditory (Elbert et al. 2002; Stevens and Weaver 2005; Gougoux et al. 2009; Schepers et al. 2012; Hertrich et al. 2013; Watkins et al. 2013) and somatosensory (Pascual-Leone and Torres 1993; Roeder et al. 1996; Sterr et al. 1998a; Sterr et al. 1998b) cortices were reported to show altered (mostly increased) neuronal activity during task processing. Intramodal plasticity has been related to early postnatal sensory experiences shaping the functional development of cortical representations as shown in animal research (Zhang et al. 2001; for review: Rauschecker 2008). For instance, reorganization of primary somatosensory and auditory areas has been reported in cats that were visually deprived

from birth (Rauschecker et al. 1992; Korte and Rauschecker 1993). Although these behavioral and neuronal adaptations have been observed, the mechanisms underlying visual deprivation-related plasticity are still poorly understood.

Studying brain rhythms in congenitally blind individuals might provide further insights into the mechanisms of neuronal plasticity, as brain rhythms reflect neuronal circuitry activity and have been related to various sensory, motor and higher-cognitive processes, as discussed in the following. Brain rhythms are thought to reflect the synchronization (phase-alignment) of oscillatory activity across neuronal populations, subserving the formation of both local assemblies and large-scale functional networks (Engel et al. 1992; Hipp et al. 2011; Raichle 2011; Siegel et al. 2012; Singer 2013). Specific spectral profiles have been conjectured to be associated with different anatomical areas (Giraud et al. 2007; Keitel and Gross 2016). Such spectral profiles are assumed to reflect the intrinsic brain rhythms of a brain area that are related to distinct processes (Keitel and Gross 2016). Importantly, intrinsic brain rhythms measured spontaneously (e.g., ongoing activity during resting state) reflect the functional organization of the brain and thus the default architecture recruited during task-related processes (Smith et al. 2009; Deco et al. 2011; Raichle 2011; Engel et al. 2013; Raichle 2015; Keitel and Gross 2016; Sormaz et al. 2018) because intrinsic brain rhythms oscillate in a characteristic way even when not involved in task-related processing (Brookes et al. 2011; Deco et al. 2011). For example, Keitel and Gross (2016) have shown that a characteristic pattern of delta-, theta-, alpha-, and beta-band activity is present in primary auditory cortex both during rest and speech comprehension. While the global appearance of the spectral profile of primary auditory cortex was similar during speech comprehension and rest, the relative contribution of individual frequency clusters (i.e., their spectral power) was altered by the condition. During speech comprehension, in comparison to rest, the alpha band was suppressed, indicating reduced inhibition of sensory cortices

1 (Jensen and Mazaheri 2010). The other bands, which were associated with several levels of

2 speech processing, were enhanced.

3 Various studies have observed that brain rhythms are recruited in a task-specific manner during

4 sensory, motor and higher-cognitive tasks, linking intrinsic brain rhythms to cognitive functions

5 (Engel et al. 1992; Singer and Gray 1995; Engel et al. 2001; Lakatos et al. 2008; Holcombe

6 2009; Giraud and Poeppel 2012; Lakatos et al. 2013; Heusser et al. 2016; Portoles et al. 2018;

7 Rimmele, Gross, et al. 2018; Schroeder et al. 2018; VanRullen 2018). For instance, in sighted

8 individuals, the role of the alpha rhythm (~8–12Hz) in cognition is well-established, with pos-

9 terior alpha- and gamma-band oscillations coupling in excitatory-inhibitory cycles (Klimesch

10 et al. 2007; Buffalo et al. 2011; Jensen et al. 2012). Specifically, the alpha rhythm mediates the

11 inhibition of task-irrelevant neuronal circuits. Gamma-band oscillations (30–100 Hz) in occip-

12 ital cortex, by contrast, allow for feedforward processing of task-relevant visual information

13 (van Kerkoerle et al. 2014; Michalareas et al. 2016). In congenitally blind individuals, a reduced

14 or absent occipital alpha rhythm has repeatedly been observed (Adrian and Matthews 1934;

15 Noebels et al. 1978; Kriegseis et al. 2006; Hawellek et al. 2013; Schubert et al. 2015). The lack

16 of visual input during a sensitive period of brain development in congenitally blind individuals

17 presumably results in atrophy or reorganization of posterior alpha generators (Ptito et al. 2008;

18 Wang et al. 2013; Aguirre et al. 2016; Reislev et al. 2016). Posterior alpha generators have been

19 located within the cortical and thalamo-cortical visual pathways (Lopes da Silva 1991; Lőrincz

20 et al. 2009) and posterior gamma generators within the cortical visual pathways (Bastos et al.

21 2014; Marshall et al. 2018). Beyond the occipital brain rhythms, however, no clear hypothesis

22 linking brain rhythms and structural alterations in congenitally blind individuals can be made.

23 In sighted individuals, beyond the alpha rhythm, intrinsic theta-band oscillations (~4–7 Hz) in

24 auditory cortex (Lakatos et al. 2005; Keitel and Gross 2016) have been widely studied. Theta

25 brain rhythms likely play a central role in the temporal segmentation of speech signals during

speech comprehension (Luo and Poeppel 2007; Giraud and Poeppel 2012; Gross et al. 2013; Doelling et al. 2014; Pittman-Polletta et al. 2020), as well as segmentation of music and environmental sounds (Henry et al. 2014; Doelling and Poeppel 2015). Interestingly, initial findings have linked the ability of congenitally blind individuals to comprehend ultra-fast speech–at rates where speech comprehension fails in sighted individuals–to accelerated theta brain rhythms in auditory cortex, as well as the recruitment of additional brain areas such as the visual cortex (Trouvain 2007; Hertrich et al. 2009; Dietrich et al. 2013; Hertrich et al. 2013; see also: Van Ackeren et al. 2018). Furthermore, initial research suggests that other brain rhythms in brain areas outside of visual cortex might also be altered in congenitally blind compared to sighted individuals (e.g., such as the beta- and gamma-band rhythm during working memory or semantic categorization tasks, as indicated by functional connectivity measures: Schepers et al. 2012; Gudi-Mindermann et al. 2018; Rimmele et al. 2019). However, the mechanisms underlying these spectral alterations remain to be elucidated. In summary, the systematics of how spectral profiles outside of visual cortex are altered due to congenital visual deprivation, are not well understood and no clear hypothesis can be derived beyond the occipital alpha rhythm.

The goal of the present study is to characterize alterations in spectral profiles in congenitally blind as compared to sighted individuals in order to map visual deprivation-related spectral changes to brain areas. By studying a broad range of frequencies, instead of narrow frequency bands, our research provides the means towards linking changes in spectral profiles across the whole brain to adaptive behavior in congenitally blind individuals in future research. Standard analyses of brain rhythms face several problems (see Keitel and Gross 2016), which possibly explains the lack of a comprehensive account of spectral changes in congenitally blind individuals beyond the alpha rhythm. Predominant neuronal activity in the alpha and super-low frequency ranges (1/f) complicates the analysis of spectral properties in the lower frequency ranges. Furthermore, the brains' temporal dynamics are often captured poorly over the course

of the recording session (de Pasquale et al. 2010; Singer 2013). Here, we have employed a novel analysis pipeline, introduced by Keitel and Gross (2016), which reveals brain area-specific spectral profiles. The analysis pipeline overcomes the limitations of standard analyses of brain rhythms by using segment-based clustering (of source-localized Fourier spectra) to disentangle spectral properties in the lower frequency ranges and by taking the time course of activity into account. We extended the pipeline (Fig. 1) to quantify differences in spectral profiles across cortical brain areas between congenitally blind and sighted individuals by using a cross-classification approach. This approach allowed us to identify brain areas with changed spectral profiles as a result of congenital blindness. More specifically, the clustering procedure reveals multi-dimensional spectral profiles that might consist of several clusters reflecting distinct intrinsic brain rhythms.

First, we expected to replicate Keitel and Gross (2016) by showing that spectral profiles in sighted adults are region-specific, enabling the classification of brain regions based on spectral profiles. Second, we hypothesized that within a group of congenitally blind individuals, spectral profiles would similarly follow specific patterns and enable the classification of brain regions. Third, visual deprivation-related plasticity was predicted to result in altered spectral profiles in congenitally blind individuals as compared to the sighted, particularly for brain regions for which visual deprivation-related reorganization (cross- and intra-modal plasticity) has previously been shown, such as for sensory cortices. A specific hypothesis regarding the changes in brain rhythms in congenitally blind individuals was only derived for the alpha rhythm, which was expected to be reduced in occipital cortex. Finally, we expected a relationship of microstructural white matter properties and spectral profiles of occipital cortex.
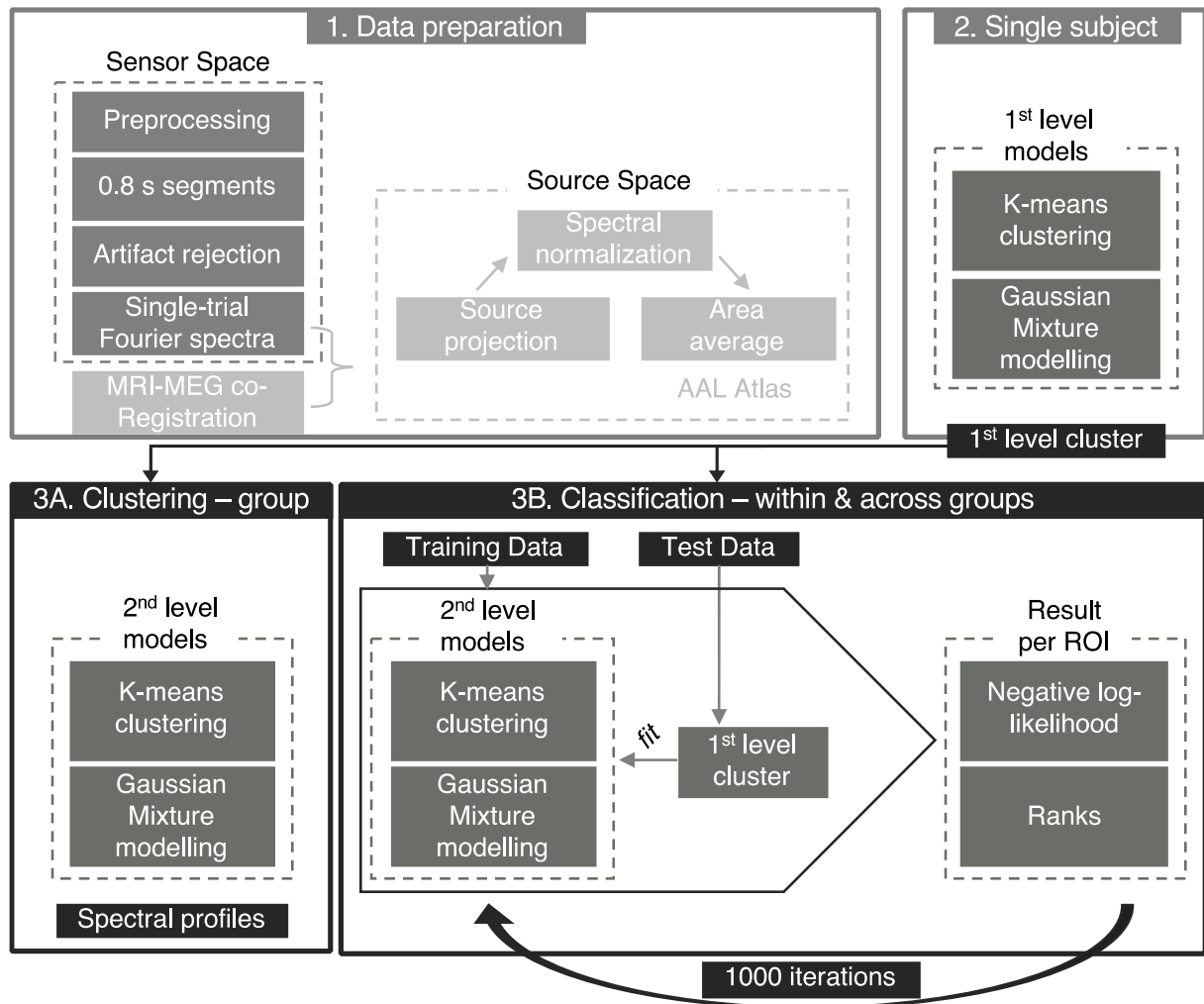
Figure 1. Analysis pipeline adapted from Keitel and Gross (2016)**.** (1) Continuous resting state MEG data were preprocessed and segmented into trials of 0.8 s length. Complex Fourier spectra were computed for each trial separately and projected into source space using previously defined beamforming (LCVM) coefficients. The data were spatially normalized, dividing each voxel's power by the mean power of all trials and voxels. Voxels were grouped according to the AAL atlas and power values were averaged across voxels of each anatomical area (N = 115). (2) In the 1st-level analysis, power matrices were clustered into 9 distinct spectral clusters per participant and brain region using k-means and Gaussian Mixture model algorithms. (3A) In the 2nd-level analysis, 1st-level individual clusters were again subjected to k-means clustering and GMMs to establish region-specific spectral clusters consistent at the group level, also referred to as spectral fingerprints. The optimal number of group-level clusters per anatomical area was defined by the Silhouette Criterion prior to the group-level clustering procedure. (3B) For the classification procedure the experimental group was divided into training and test set. For each brain region, the fit between 1st-level clusters of the test group and group-level clusters of all regions of the training set was calculated. For each anatomical region, this resulted in a negative log-likelihood value for all regions (i.e., 115 values per region), indicating its similarity to all brain regions based on the spectral clusters. This fitting procedure between training and test set was repeated 1000 times with new group assignment (training vs. test) on each iteration. The interindividual variance within test and training groups of each iteration was controlled for with an additional 100 iterations within the respective sets.

1 Materials and Methods

2 Participants

The study was approved by the German Psychological Association. All participants gave written informed consent prior to the experiments and received monetary compensation. The data were recorded in the context of a larger project (Gudi-Mindermann et al. 2018; Rimmele et al. 2019). Three to four minutes of resting state MEG data were collected from a group of sighted and congenitally blind individuals matched in age, gender and education. During data collection the congenitally blind (CB) and the sighted (S-BF) participants were blindfolded. The blindfolding of CB participants aimed at reducing involuntary eye movements. Additionally, for the sighted a resting state measurement with open eyes was conducted (S-EO). The data reported here include (after a few subjects were excluded, see below) 26 subjects for the CB (12 females; mean age: 37.8 years; *SD*: 10.2 years; age range: 22–55 years), 24 for the S-BF (11 females; mean age: 36.8 years; *SD*: 10.1 years; age range: 21–55 years) and 23 for the S-EO (11 females; mean age: 37.3 years; *SD*: 9.8 years; age range: 21–55 years). A few subjects were excluded after data collection because of corrupted resting state files (one subject for the CB, one subject for the S-EO) or lack of individual structural MRI scan (three subjects for the S-BF and S-EO). All participants were healthy with normal hearing (self-report) and assured no history of psychiatric or neurological disorders. One blind participant reported a history of a depressive mood disorder, but was free of symptoms and without current treatment. Sighted participants had normal or corrected-to-normal vision (self-report). In the blind, vision loss was total and resulted from a variety of peripheral (pre)natal conditions (retinopathy of prematurity: $n=9$; genetic defect, $n=5$; congenital optic atrophy: $n=2$; Leber's congenital amaurosis: $n=2$; congenital cataracts, glaucoma: $n=2$; congenital retinitis: $n=2$; binocular anophthalmia: $n=2$; retinitis pigmentosa: $n=1$; congenital degeneration of the retina, $n=1$). Seventeen participants reported minimal residual light perception.

MRI and MEG Data Acquisition

For all participants T1-weighted structural MRI scans and DWI-MRI scans were obtained with a 3T scanner (Siemens Magnetom Trio, Siemens, Erlangen, Germany). For the T1-weighted images we used the following parameters: TE = 2.98 ms, TR = 2300 ms, flip angle = 9, and isotropic 1 mm3 voxels, 256 sagittal slices. The MEG data were recorded in a magnetically shielded room using a 275-channel whole-head system (Omega, 2000, CTF Systems Inc.), while participants sat in an upright position. The data were acquired with a sampling rate of 1200 Hz. Prior to each experiment, the head position was measured relative to the MEG sensors and during the recording the head position was tracked.

Data Analysis

The initial analyses in this study are adopted from the analysis pipeline proposed by Keitel and Gross (2016). The modifications to the analysis pipeline and the novel analyses are stated in detail below. All analyses were carried out using Matlab R2018a (version 9.4.0.813654, The Math Works, Inc.), the Fieldtrip Toolbox (version 20181104), and SPM12.

Data Preparation in Sensor Space: Preprocessing, Artifact Rejection, Source Localization

During preprocessing, the MEG signal was downsampled to 250 Hz, denoised and detrended. To better capture the dynamically changing spectral properties of the brain, the continuous signal was segmented into trials of 0.8 s. Trials were declared as noisy and excluded when their z-score was higher than 2. On average, seven trials were excluded, resulting in a mean of 340.3 trials (*SD*= 34.7) per subject (S-EO: mean = 346.7, *SD* = 37.4; S-BF: mean = 336.8, *SD* = 34.2; CB: mean = 338, *SD* 33.2). Due to shorter recordings in the present study, trial duration was slightly shorter, relative to the 1 s duration used in Keitel and Gross (2016), to increase the amount of trials. MEG channels were labeled as noisy and rejected when the ratio between their noise level (in *SD*) and that of the neighboring sensors (in *SD*) exceeded a value of 0.5 ([Sensor

1   *SD* – Neighbor *SD*] / Neighbor *SD*; mean number of excluded channels = 1.22, *SD* = 1.34).

2   Finally, using independent component analysis (ICA), data was cleaned from heartbeat, eye

3   blinks and eye movements-related artifacts (components were identified based on their time-

4   course, topography and variance across trials). To prepare the source projection of the Fourier

5   spectra, beamformer coefficients were obtained. For this purpose, we applied co-registration of

6   individual T1-weighted MRI scans and the MEG coordinate system, realignment, segmentation

7   and normalization to Montreal Neurological Institute (MNI) space. A forward model was cre-

8   ated using a single-shell model and linearly constrained minimum variance (LCMV) beam-

9   former coefficients (Van Veen et al. 1997) were calculated for the MEG time series for each

10   individual voxel on the 10 mm regular grid.

11   **Spectral Analysis in Sensor Space**

12   The analyses described in the following were performed for all three groups separately (CB, S-

13   EO, S-BF; for an overview, see Fig. 1). First, Fourier spectra were calculated on 0.8 s long trials

14   for each subject, using a multitaper approach (3 tapers) and zero-padding (length of 2 s). We

15   slightly reduced the duration of the temporal segments compared to the duration used by Keitel

16   and Gross (2016), i.e., 1 s, in order to match the overall number of segments used for the anal-

17   yses while accounting for the shorter overall MEG recording time in our study. Second, using

18   the previously computed LCMV coefficients, the complex Fourier spectra were projected into

19   source space. Neuronal power, i.e., the squared amplitude of the Fourier coefficient, was com-

20   puted for each time segment, voxel, and frequency. Furthermore, neuronal power of individual

21   voxels and segments was ratio normalized, i.e., divided by the mean power across all voxels

22   and trials. This ratio normalization resulted in voxel-specific spectral properties with values

23   above/below 1 highlighting the differences of a given voxel to the mean spectral power across

24   all voxels separately at each frequency. All values were subtracted by 1 (leading to values

25   above/below zero), to facilitate the identification of changes in power (decreases/increases). We

additionally conducted a control analysis without the normalization by performing the cluster-ing and classification procedures on the non-normalized data.

k-Means Clustering and Gaussian Mixture Modelling of Source-Localized Spectral Ac-tivity

To identify region-specific spectral clusters in the individual subject, the brain was parcellated according to the AAL atlas (Tzourio-Mazoyer et al. 2002; 116 regions of interest, ROIs). For one anatomical region (cerebellum 3L), however, the interpolation between the AAL atlas and the source model was not successful. Thus, this region was excluded and all analyses are based on the remaining 115 anatomical areas. For each of the ROIs, voxels were grouped and power spectra were averaged across voxels. Within a brain area, neuronal populations might express several distinct intrinsic brain rhythms, which together constitute the spectral profile of an area. Clustering algorithms were employed to identify spectral clusters, reflecting intrinsic brain rhythms. First, trial-by-frequency matrices were subjected to a k-means algorithm (MacQueen 1967) which established spectral clusters by partitioning the n observations (0.8 s temporal segments) into k clusters. For the 1st-level analysis, the k was set to 9, based on the Silhouette criterion evaluation (Rousseeuw 1987). Second, for each subject and ROI, Gaussian Mixture Models (GMMs; Reynolds and Rose 1995) were fitted to the 9 clusters obtained from the k-means analysis (1st-level GMM). Next, in order to identify the optimal number of clusters per brain region across all subjects for the 2nd-level group analysis, the 1st-level GMMs were eval-uated using the Silhouette criterion. Silhouette values were computed for cluster solutions in the range from 1 to 15, the fitting was repeated 1000 times. At the group level, k-means clus-tering was applied to the 1st-level clusters in order to disclose consistent patterns across subjects. The optimal number of clusters per brain area, as assessed by the Silhouette criterion evaluation (Rousseeuw 1987), was used as k-parameter for the algorithm. As before, k-means results were fed into GMM revealing the final clusters per brain region (2nd-level GMM).

Clusters were considered for visualization only if they were reflective of the majority of participants. To facilitate reading of the spectral plots, group-level clusters were color-coded according to the frequency of the maximum amplitude of the cluster (peak frequency) (delta: 1–3.5 Hz, red; theta: 4–8 Hz, green; alpha: 8.5–12.5 Hz, blue; beta: 14–30.5 Hz, yellow; gamma: 33.5–100 Hz, magenta). Furthermore, we computed the relevance of each cluster per brain region by analyzing the amount of single subject trials during which a cluster was present. Group clusters (Fig. 1, step 3) were traced back to single subject clusters and the amount of trials that contributed to a single subject cluster (Fig. 1, step 2) was calculated and expressed as percentage. Percentages were averaged across subjects.

Automatic Within-Group Classification

A classifier was employed to test the specificity of region-specific spectral fingerprints. After splitting each group into half (training and test group), group-level clusters were calculated for the training group for all anatomical regions using k-means and GMM clustering. For each brain region and participant of the test group, the similarity of spectral profiles was assessed as compared to all brain regions of the 2nd-level group clusters of the training group by computing the negative log-likelihood for all pairs of regions. This procedure, i.e., group assignment and classification, was repeated 1000 times (note that for the S-EO one subject was left out in every iteration to yield an even number of participants in training and test groups). On each iteration, an additional loop ($N = 100$) controlled for interindividual noise within a group by randomly drawing the adequate number of subjects (i.e., $N_{S-EO} = 11$, $N_{S-BF} = 12$, $N_{CB} = 13$) from the group with replacement, allowing a subject to enter multiple times or not at all. Put differently, within one iteration ($N = 1000$) each participant belonged to either the training or the test group. To account for individual differences, the group clusters were calculated 100 times with a different subset chosen from the respective group each time and finally averaged to obtain a robust group

1 estimate. Based on the mode of clusters identified per brain region in the 2nd-level cluster anal-

2 ysis, the optimal number of clusters for the classification analysis was $k = 2$. Likelihood values

3 were ranked and averaged across iterations (20% trimmed mean). For further comparisons, only

4 corresponding ROIs (e.g., how is the Heschl ROI in the test set ranked based on the training set

5 Heschl ROI) were considered.

6 In addition to the descriptive report of the classification performance, here we tested whether a

7 specific ROI (of the test set) was classified significantly better by the corresponding area of the

8 training set as compared to all other 115 ROIs. This allowed us to exclude the possibility that

9 classification performance was caused by unspecific effects—that is, generic fingerprints. To

10 this end, each region's mean rank (averaged across iterations) was tested against a distribution

11 of classification ranks generated from all other ROIs (null distribution).

Automatic Cross-Group Classification

13 In order to identify differences in region-specific spectral properties between the CB and S-BF,

14 we performed a cross-group classification. We employed the same classification procedure as

15 before; however, the classifier was trained on one group (S-BF), while the other (CB) was uti-

16 lized as the test set. As before, the classification procedure was repeated 1000 times, drawing a

17 subset of $N = 12$ per group on every iteration. The randomization of subjects chosen on each

18 iteration was identical to the one used for the within-group classification in the S-BF (this is the

19 reason why $N = 12$, instead of using all subjects of both groups). Thus, differences in the clas-

20 sification, as reflected by the ranks, could not be caused by the training set per se. In order to

21 understand whether some brain areas in the CB were not classified well based on the S-BF

22 spectral profiles (i.e., whether the classification of brain regions was different in the cross-group

23 condition as compared to the within-S-BF classification), we tested the cross-group classifica-

24 tion mean ranks against the distribution of ranks from the same ROI from the S-BF group (here

25 the null distribution). The distributions were generated by taking the classification rank of a

14

corresponding area from training and test set (i.e., Calcarine) across all iterations (see Fig. S2 for the distributions of all brain areas). We calculated the 95th percentile of the distribution and tested whether the cross-group mean rank of the current region fell above (significant) or below (not significant) this threshold.

To further assess the spectral profiles of brain areas that were significantly different in the cross-group classification, post-hoc permutation statistics were applied to the raw, normalized region-specific spectra (i.e., Fourier spectra without clustering procedure). This additional analysis was performed to evaluate the cross-group differences between the sighted and the congenitally blind groups by using a simpler, more established approach. The analysis confirmed the findings from the spectral clustering approach. The spectral analysis was calculated as in the main analysis (see above). For all significant brain regions separately, power was averaged across voxels and segments, resulting in a single power value per frequency and per subject. Based on frequency by subject matrices for the CB and the S-BF, group differences in spectral power were tested against a distribution where the group assignment (CB vs. S-BF) was randomly permuted ($N = 1000$). To control for multiple comparisons, we used FDR ($Q = 0.05$).

Microstructural White Matter Properties

DW-MRI data were acquired together with T1-weighted structural scans described above. We used an echo planar imaging (EPI) sequence optimized for DWI-MRI of white matter covering the whole brain (64 axial slices; bandwidth = 1502 Hz/Px, 104 × 128 matrix, TR, 8,200 ms; TE, 93 ms; flip angle, 90°; slice thickness, 2 mm; voxel size, $2 \times 2 \times 2$ mm3). The protocol comprised three acquisitions yielding a total acquisition time of 9 min 51 s. This resulted in a total of 120 diffusion-weighted volumes with six interleaved non-diffusion-weighted volumes (b values of 1,500 s/mm2). DWI-MRI scans were acquired from a subset of the original sample of 16 blind and 12 sighted participants.

DTI-MRI preprocessing and analysis. Diffusion data processing initially corrected for eddy current distortions and head motion by using FMRIB's Diffusion Toolbox (FDT; FMRIB Software Library; FSL 5.0.1; http://www.fmrib.ox.ac.uk/ fsl/; Jenkinson et al. 2012). For a more accurate estimate of diffusion tensor orientations, the gradient matrix was rotated to correct for head movement, using the fdt_rotate_bvecs program in FSL. We then used the Brain Extraction Tool (Smith 2002) for brain extraction, also part of the FSL distribution. Analysis continued with the reconstruction of the diffusion tensors using FSL's DTIFIT program. FA and RD maps for each participant were calculated using the eigenvalues extracted from the diffusion tensors. Note that FA maps are required in the early stages of TBSS to compute the registrations to MNI standard space and subsequently create the diffusion skeletons. However, we focused our analysis on RD, as this is a more specific measure of diffusivity in white matter than FA or mean diffusivity. Indeed, although several factors can contribute to producing particular RD values, including the number of axons and axon packing and diameter, RD has been most consistently related to myelin content along axons, with increased RD values reflecting higher demyelination (Song et al. 2002; Song et al. 2005; Klawiter et al. 2011; Zatorre et al. 2012). In animal studies, directional measures such as RD, unlike summary parameters such as mean diffusivity or FA, provide better structural details of the state of the axons and myelin (Aung et al. 2013).

Voxel-based analyses of RD maps were performed with TBSS (Smith et al. 2006). Participants' FA maps (necessary to calculate the registrations to MNI standard space and create the RD skeletons) were registered to the FMRIB58_FA template (MNI152 space and $1 \times 1 \times 1$ mm3) using the nonlinear registration tool (Andersson et al. 2007). These registered FA maps were first averaged to create a mean FA volume. A mean FA skeleton was then produced, representing the centers of all white matter tracts common to all participants in the study. Each participant's aligned FA data were then projected onto this skeleton by searching for the highest FA value within a search space perpendicular to each voxel of the mean skeleton. This process was

repeated for the RD maps by applying the transformations previously calculated with the FA maps. This resulted in individual RD skeletons for each participant. Finally, to assess white matter differences between CB and sighted participants, independent-samples t-tests were performed on the RD skeleton. Significant results are reported at FWE-corrected $p < 0.05$ using threshold-free cluster enhancement (Smith and Nichols 2009) and a nonparametric permutation test with 5,000 permutations (Nichols and Holmes 2002). Significant cluster results were averaged and a mean value per participant, reflecting individual microstructural differences, was obtained.

For the mapping between RD values and the standard probabilistic atlases of white matter pathways, all voxels that differed significantly in RD values between the CB and sighted were included. We report only tracts that showed an overlap with these voxels, with the tracts from the probabilistic atlas thresholded at 0.95 probability.

Spearman correlations were used to analyze the correlation between RD values (across groups) and the spectral profiles of brain areas in the occipital cortex. For these areas, peak power values were retrieved for all clusters (i.e., lines showing clear power peak) of the complex spectral profile for each subject, and correlated with the RD values. Multiple comparisons were controlled for by using FDR (Q = 0.05).

Results

Spectral Fingerprints Replicate

In our sample of sighted adults with open eyes we successfully replicated the classification of individual brain regions by their spectral profiles as first reported by Keitel and Gross (2016). Particularly, for all tested 115 ROIs the mean classification performance, indicated by the classification ranks, was high (Fig. 2A). Classification ranks refer to the probability of a region being identified by the classifier: For example a mean rank of 1 indicates that a region was

correctly assigned (i.e., highest probability among all areas) on every iteration; a mean rank of

2 means that the assignment was correct in many but not all of the iterations (i.e., had the second

highest probability among all areas). Here, the mean rank (averaged across all iterations and

brain areas) obtained from the classifier analysis was 2.70 (range of ranks: 1–12.7, Keitel mean

rank = 1.8), or 2.32 when considering identification of the homologue (left/right hemisphere)

areas as a hit (Keitel homologue mean rank = 1.4). Mean ranks of all ROIs are depicted in the

histogram and surface plot in Fig. 2A. We statistically quantified the classification performance

using permutation tests. The mean classification rank of an area (e.g., right calcarine) was tested

against a distribution of classification ranks of all brain areas (except the current one, e.g., right

calcarine) accumulated across all iterations ($N = 1000$). For an area with a characteristic spectral

profile, classification between corresponding areas (e.g., right calcarine in training vs test set)

should be best and thus fall above the 95th percentile of the generated null-distribution. This

analysis revealed that for 97% of all areas classification was significantly better when identify-

ing themselves compared to all other regions.
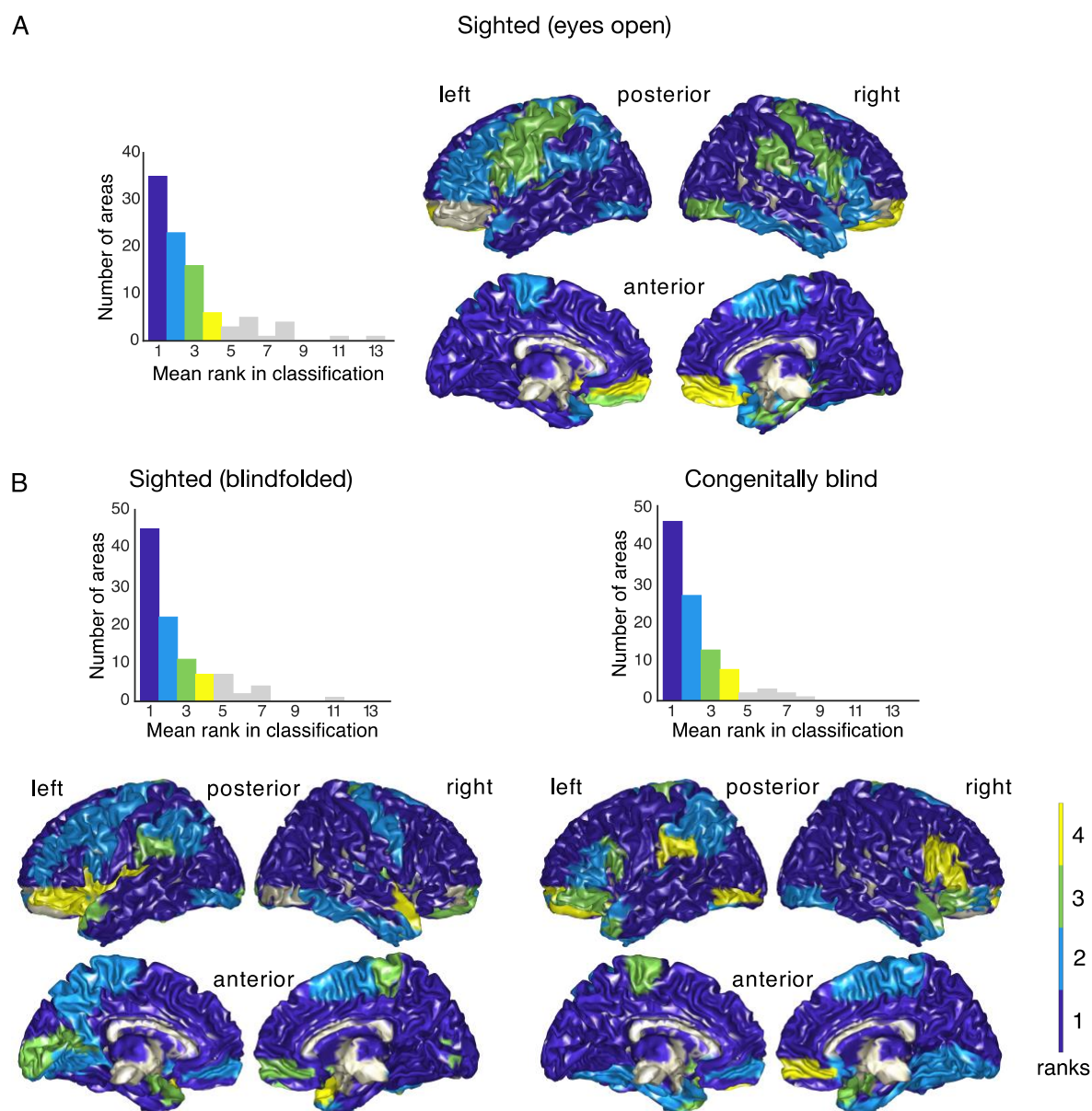
Figure 2. Classification results for all experimental groups. (A) Sighted group with open eyes (replication sample). *Left.* Histogram of mean ranks in classification across all 115 brain areas. 84.5% of the brain regions obtain a mean rank between 1 and 4, while 15.5% of regions were assigned ranks up to 13. (in Keitel and Gross (2016) all mean ranks were between 1 and 4). *Right.* Topography of mean ranks (colors match ranks from the histogram). **(B) Sighted group with eyes closed (*left*) and group of congenitally blind individuals (*right*).** For both groups, the histogram of mean ranks in classification across all 115 brain areas is displayed in the upper panel and the topography of mean ranks (colors match ranks from histogram) is displayed in the lower panel. Bin width is 1 for all subplots.

Furthermore—although the average optimal number of clusters per anatomical area was lower

in our sample (3.4 +/– 2.3 clusters per area (see Fig. 4 and Fig. S1, Supplementary Data) vs. 4.1

+/– 1.86 (*M + SD*) in Keitel and Gross (2016)—the clustering approach revealed comparable

spectral fingerprints between the studies. Interestingly, for deeper subcortical brain structures

19

1 (e.g., thalamic and limbic areas), the clusters were less characteristic in the present data (i.e.,

2 only a few clusters per area with less specific shapes and high classification ranks; see Fig. S1),

3 possibly reflecting limitations of the signal-to-noise ratio of the used MEG system.

4 **Good Classification Within Sighted and Congenitally Blind Groups**

5 Our second hypothesis stated that, within a group of congenitally blind individuals, anatomical

6 areas are characterized by specific (although possibly altered as compared to the sighted) spec-

7 tral fingerprints. We performed the classification procedure for the CB and observed good clas-

8 sification ranks (similar to the ones observed for the S-EO; Fig. 2B; mean rank = 2.51, range =

9 1–10.3, homologue mean rank = 2.10, percent significant ROIs = 100%), indicating consistent

10 spectral clusters of brain areas in congenitally blind participants. The same procedure was per-

11 formed on the data of the S-BF and revealed similarly good classification ranks (S-BF: mean

12 rank = 2.64, range = 1–11.4, homologue mean rank = 2.17, percent significant ROIs = 98%) as

13 compared to the S-EO and CB.

14 Ensuring good within-group classification in the CB and the S-BF was an important prerequisite

15 for consecutive between-group analyses as it promised to prevent potential group differences

16 from arising from large within-group variance. Furthermore, the results showed a similar dis-

17 tribution of mean ranks across the cortical surface for both the CB and the S-BF group, such

18 that the majority of brain regions (~70 out of 115) was identified as best or second-best.

19 **Spectral Changes in Sensory and Right Frontal Regions in Congenitally Blind Individuals**

20 Based on the literature on intra- and cross-modal plasticity in the CB, we hypothesized that

21 spectral properties would differ between the congenitally blind and normally sighted individu-

22 als. To test if (and which) brain areas differed in their spectral properties between the two

23 groups, we implemented a cross-group classification drawing samples from the S-BF for the

1   training and samples from the CB for the test group. This analysis resulted in a mean rank of

2   5.3 (range = 1.09 - 27.17) (Fig. 3A).
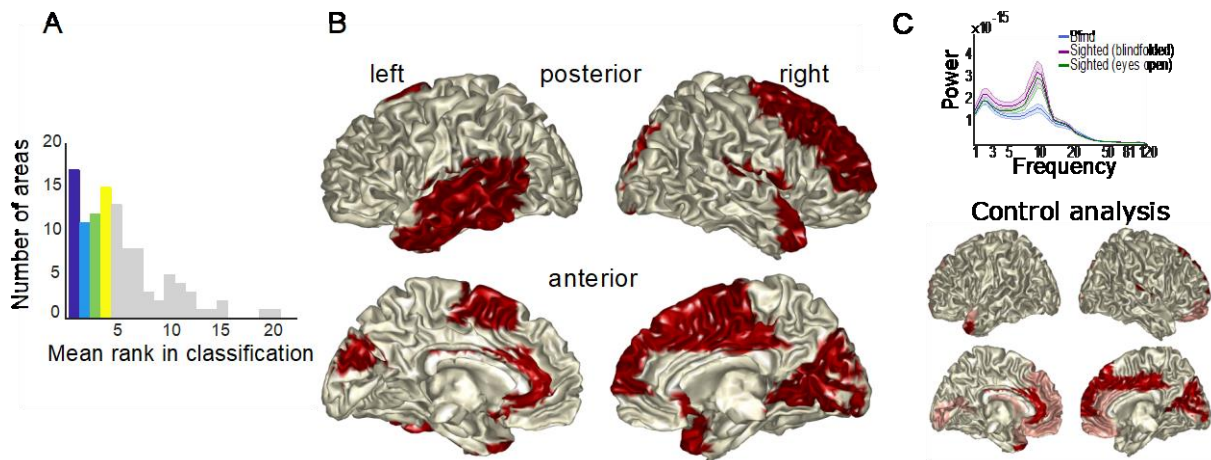
4   **Figure 3. Cross-group comparison**. (A) Histogram of classification ranks. Bin width is 1. (B) The topographic
5   distribution of significantly different classification ranks in the cross-group classification is highlighted in red, as
6   tested by a permutation procedure. (C) The normalization spectrum used in the normalization procedure (i.e., the
7   average power spectrum across segments and voxels) is displayed, averaged across participants, separately for
8   each experimental group (upper panel). Shaded error bars reflect the standard error of the mean across participants.
9   Frequency is displayed at the x-axis, scaled logarithmically from 1 to 120 Hz; power on the y-axis. For visualiza-
10   tion, power was interpolated at 50 Hz to remove line noise. In order to test the impact of the normalization proce-
11   dure on our cross-group classification findings, a control analysis on the non-normalized data was performed
12   (lower panel). Confirming our findings, the control analysis revealed significant findings in various areas overlap-
13   ping with the areas observed in the main analysis (highlighted in dark red). However, we also observed several
14   additional areas with significant group differences (highlighted in light pink), as well as areas that, in contrast to
15   the main analysis, did not show significant group differences in the control analysis (see Table S2 for a full list).
16   Only findings at brain areas that showed group differences in both, the main cross-group and the control analyses
17   (i.e., with and without normalization procedure) will be considered for discussion.

19   In the cross-group analysis, 54.8% of 115 areas obtained classification ranks ranging from 1 to

20   4, while the automatic identification of the remaining regions was less precise (see Fig. 3A).

21   Beyond these descriptive procedures, we statistically compared classification results in the

22   cross-group condition as compared to the within S-BF group classification (see Fig. S2 for the

23   distributions of all brain areas). As seen in Fig. 3B, cross-group classification ranks were sig-

24   nificantly worse for several sensory as well as for right frontal areas, and an extended network

25   of left temporal brain regions. This suggests that spectral profiles in these brain regions were

26   different in the CB group as compared to the sighted (see Table 1 for all ROIs showing signif-

icantly worse classification compared to the null-distribution). A control analysis was per-

formed, to assure that group differences were not introduced by the normalization procedure

(i.e., reflecting differences in baseline power, Fig. 3C). While this analysis largely confirms our

findings, some of the brain areas did not show significant group differences in the control anal-

ysis and several additional areas with significantly worse classification ranks were found (see

Table S2 for a full list). Differences between the analyses are partly reflecting the advantages

of the normalization procedure, i.e., that it down-weights the neuronal activity (1/f power) that

is predominant across the brain and not specific to a given brain area (Fig. S5). In the following,

we focus on the interpretation of findings at ROIs that showed significant group differences in

both cross-group classification analyses (i.e., with and without normalization procedure). These

areas comprise: right Heschl's gyrus, Calcarine gyrus, Cuneus, superior medial frontal gyrus,

middle cingulate cortex and left middle temporal pole and anterior cingulate cortex (highlighted

in Table 1).

| Coarse region	Hemisphere	
	Left	**Right**
Frontal		Superior frontal gyrus
		Middle frontal gyrus
		Superior medial frontal
		Rolandic Operculum
Visual	Cuneus	**Calcarine gyrus**
		Cuneus
		Superior occipital gyrus
		Lingual gyrus
Temporal	Superior temporal gyrus	**Heschl's gyrus**
	Middle temporal gyrus	Middle temporal pole
	Middle temporal pole	Superior temporal pole
	Inferior temporal gyrus	
Sensorimotor	Supplementary Motor Area	Supplementary Motor Area
Non-cortical	Olfactory	Olfactory
	Anterior cingulate cortex	**Middle cingulate cortex**
	Cerebellum lobule VI	Cerebellum lobule X
	Cerebellar vermis 3	Cerebellar vermis 3
	Cerebellar vermis 9	Cerebellar vermis 9

Table 1. Table of all brain areas (out of 115) with significant classification differences. Brain areas where classification ranks were significantly different between the congenitally blind and the sighted (blindfolded) are listed. The areas highlighted in bold showed significant group differences in the cross-group classification analyses

1 (i.e., with normalization procedure) and in the control analysis (i.e., without normalization procedure; see Fig. S5)
2 and will be the focus of interpretation.

3

4 Interestingly, the brain areas identified as showing group differences in the spectral profiles in

5 the cross-group classification were characterized by clusters comprising peaks with increased

6 power at higher frequencies in the CB as compared to the S-BF participants (for an exemplary

7 selection of brain areas with significant effects, see Fig. 4A; spectra of all brain areas are shown

8 in Fig. S1). This pattern of results was observed for the auditory (with more power in the alpha

9 and beta band in the CB as compared to the sighted participants) and the right frontal areas

10 (more power in the theta band). In visual brain areas, power peaks were reduced in the alpha

11 band for the CB as compared to the S-BF participants, in contrast, power was increased in the

12 low-gamma band. Post-hoc permutation tests were performed to confirm these observations.

13 To test differences in spectral signatures between the S-BF and CB, the raw Fourier spectra

14 (i.e., without applying the spectral clustering) were extracted und subjected to permutation sta-

15 tistics. Participants' group assignment (S-BF vs. CB) was permuted randomly (1000 permuta-

16 tions) (Q = 0.05; false discovery rate [FDR] corrected p-value = .033; p-values < .033) (see Fig.

17 4B and Fig. S3). Although the differences in low-gamma power in the calcarine between the

18 CB and the S-BF were not significant in the post-hoc tests, see Fig. S6.
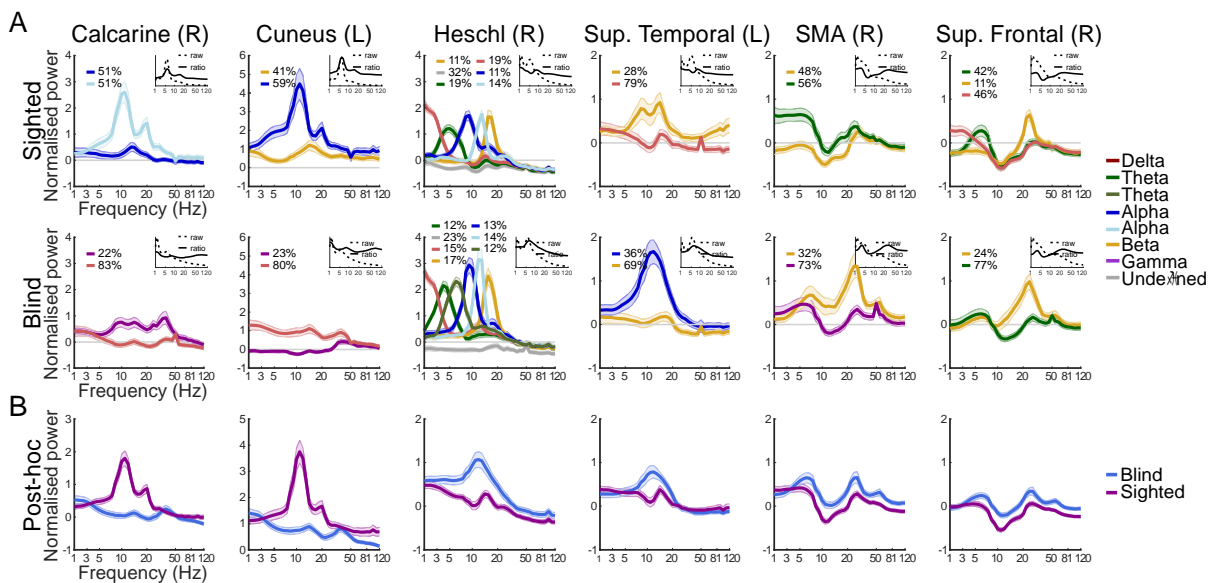
19

1 **Figure 4. Comparison of spectral profiles of sighted and blind participants**. (A) A selection of the spectral
2 profiles of the brain areas (columns) that showed significantly worse cross-group classification is displayed, sep-
3 arately for the S-BF and the CB (rows). Clusters are color-coded according to the frequency of the cluster ampli-
4 tude peak (legend on the right). The insets display the normalized mean power spectra (solid lines) and the unnor-
5 malized mean power spectra (dashed lines) (i.e., both without applying the spectral clustering). (B) Post-hoc anal-
6 yses of the spectral differences are displayed for the selection of brain regions (columns). Spectra represent nor-
7 malized mean power spectra (i.e., without applying the spectral clustering) at each ROI. Frequencies where power
8 differences were obtained between the groups are indicated by grey boxes (permutation test: Q = 0.05; FDR cor-
9 rected p-value = .033; p-values < .033). The groups are color-coded (legend on the right). In all panels: Shaded
10 lines indicate standard error of the mean.

11

12 **Spectral Changes Correlate with Structural Group Differences**

13 In order to test the relation of occipital spectral differences between the groups observed in the

14 classifier analyses and their relation to brain structure, we performed a diffusion-tensor imaging

15 (DTI) data analysis for a subsample of participants. The TBSS analysis revealed significantly

16 higher Radial Diffusivity (RD) values in a bi-hemispheric spatial cluster in posterior parts of

17 the brain (i.e., a cluster of voxels; displayed in Fig. S4B) for the CB as compared to the sighted

18 participants ($N_{sighted} = 12$, $N_{CB} = 16$; family-wise error (FWE)-corrected at the peak voxel,

19 two-sided p = 0.05; see Fig. S4B), indicating reduced white matter structural integrity in the

20 CB group. We used a probabilistic atlas of white matter pathways in MNI space (Thiebaut de

21 Schotten et al. 2011) to evaluate the overlap of the spatial cluster with known white matter

22 tracts. With the probabilistic atlas thresholded at 0.95, the TBSS cluster presents a significant

23 overlap with the posterior corpus callosum, the posterior inferior longitudinal fasciculus (bilat-

24 erally), the posterior inferior fronto-occipital fasciculus (bilaterally), and the optic radiations

25 (also bilaterally). This means that there is a 95% chance that the reduced white matter properties

26 identified in the CB group by the TBSS analysis primarily affect these white matter tracts.

27 Finally, RD values belonging to this spatial cluster were extracted and correlated with the power

28 of individual cluster peaks from the spectral profile of occipital brain areas (Spearman correla-

29 tions, FDR correction, Q = 0.05, corrected *p*-value = .0065, Fig. S4C). RD correlated negatively

30 with the alpha power in right (rho = –0.55, p = .005) and left (rho = –0.81, p > 0.001) calcarine,

as well as left cuneus (rho = –0.68, *p* > .001), indicating that reduced white matter properties in occipital areas were accompanied by reduced neuronal alpha power. Alpha and gamma power of the remaining occipital regions did not correlate with the RD values (all *ps* > .0065; cf. Table S1).

Discussion

Intrinsic brain rhythms likely are involved in various sensory, motor and higher-cognitive processes. In congenitally blind individuals, behavioral performance in tasks involving the intact senses has often been found to be enhanced (Lessard et al. 1998; Roeder et al. 2000; Roeder et al. 2003; Gougoux et al. 2004; Hoetting et al. 2004; Roeder et al. 2004; Gougoux et al. 2005; Hertrich et al. 2009; Dietrich et al. 2013), and structural and functional reorganization has been observed in brain areas associated with the intact sensory systems (Pascual-Leone and Torres 1993; Sterr et al. 1998a; Sterr et al. 1998b; Roeder et al. 1999; Elbert et al. 2002; Stevens and Weaver 2005; Gougoux et al. 2009; Schepers et al. 2012; Hertrich et al. 2013; Watkins et al. 2013), as well as in brain regions predominantly associated with the visual system (Elbert et al. 2002; Burton 2003; Roeder and Neville 2003; Noppeney et al. 2005; Pascual-Leone et al. 2005; Noppeney 2007; Bedny et al. 2011; Voss and Zatorre 2012). Whether and how these behavioral and neuronal adaptations affect brain rhythms outside of occipital brain regions had remained unclear to date. Here, we identified spectral alterations in congenitally blind individuals aiming at advancing a mechanistic understanding of adaptations to blindness. Furthermore, our findings add to the ongoing debate regarding the functional relevance of brain rhythms. Confirming our first two hypotheses, spectral clustering and classification procedures performed exceptionally well for all groups (97–100% of areas were classified correctly in each group). This highlights consistent brain area-specific spectral properties across individuals within the sighted group and, as demonstrated for the first time, within the congenitally blind group. Crucially, cross-classification showed that visual deprivation co-occurred with changes in the spectral

25

1   profiles especially of sensory (auditory and visual), right-frontal, left middle temporal pole and

2   bilateral parts of the cingulate cortex. This was reflected in increased power in the theta-to-beta

3   frequency bands in the right primary auditory cortex and right-frontal brain regions. In visual

4   cortex, the sighted showed the alpha rhythm typically observed during rest, whereas in the con-

5   genitally blind individuals, clusters with expected decreased alpha power were accompanied by

6   a gamma (~40 Hz) peak, suggesting an altered inhibitory-excitatory balance in the blind. Addi-

7   tionally, a correlation analysis of individual spectral clusters in occipital cortex and microstruc-

8   tural white matter properties revealed a positive correlation between alpha (but not gamma)

9   power and white matter integrity in an extended bi-hemispheric spatial cluster in posterior parts

10 of the brain.

11 **Robust Classification of Brain Areas Based on Spectral Profiles**

12 Spectral profiles measured during resting state have revealed intrinsic brain rhythms that are

13 thought to be crucially involved in task-related processing (Smith et al. 2009; Hipp et al. 2012;

14 Engel et al. 2013; Raichle 2015; Keitel and Gross 2016; Sormaz et al. 2018). In the present

15 study, we replicated the observation that brain areas expressed characteristic spectral profiles

16 (Keitel and Gross 2016). Spectral clustering and automatic classification revealed spectral pro-

17 files, classification ranks, and distributions of classification ranks across the cortex in the

18 sighted (S-EO) group similar to the ones first reported by Keitel and Gross (2016). Spectral

19 profiles, for example of occipital regions, showed the typically observed alpha rhythm peaking

20 at ~10 Hz, which has repeatedly been found to be involved in attentional inhibition (Klimesch

21 et al. 2007; Buffalo et al. 2011; Jensen et al. 2012). Spectral peaks in the beta band (~20 Hz)

22 were prominent across frontal and central brain areas, resembling previously reported natural

23 frequencies of these brain areas (Rosanova et al. 2009; Ferrarelli et al. 2012; Keitel and Gross

24 2016), which may play a role in temporal motor processing (Fujioka et al. 2012; Arnal et al.

25 2015; Morillon and Baillet 2017).

While the spectral profiles of most brain areas resembled those reported by Keitel and Gross (2016), for some brain areas the spectral profiles differed (see Fig. S1). In our study, deep sub-cortical brain areas (in contrast to what has been reported by Keitel and Gross 2016) were not classified well (Fig. S1). A possible reason for this is that the slightly shorter segment duration used in the present study, which reduced the frequency resolution at lower frequencies, affected the detection of low-frequency clusters. Alternately, a lower signal-to-noise ratio in deeper brain areas in our data as compared to Keitel and Gross (2016) might be related to the employ-ment of different MEG systems. Thus, possibly the recording system used and/or the sample of participants tested potentially influenced the specific profiles of some brain areas more than others. A test on a large dataset across different recording sites (i.e., several hundreds of record-ings) will be necessary to clarify which spectral modes generalize across individuals of a larger population. Importantly, within our sample, the spectral profiles were consistent across individ-uals (i.e., only group clusters were reported in which at least ~70% of participants, and on av-erage ~97% for the S-EO and ~94% for the S-BF group, contributed to each of the group-level spectral clusters). In summary, our results highlight the robustness of brain area-specific spec-tral profiles, suggesting that spectral profiles are characteristic properties reflecting the intrinsic brain rhythms of cortical regions.

On the premise that changes in spectral profiles are functionally related to adaptive plasticity in congenitally blind individuals, they are expected to be consistent (and not random) within a group of congenitally blind individuals. A novel finding of our study which is in accord with this hypothesis is that in the congenitally blind group, as with the sighted group, brain regions were identified reliably based on their spectral clusters, suggesting spectral consistencies across individuals (Fig. 2B, right; i.e., only group clusters were reported in which at least ~69% of participants and on average ~95 % contributed to each spectral cluster). This result suggests

1 that adaptation of the cortex to visual deprivation leads to specifically and homogenously al-

2 tered spectral fingerprints in the congenitally blind individuals.

3 **Selective Spectral Plasticity Across the Brain**

4 The main goal of our study was a comprehensive (in space and frequency), data-driven model

5 of spectral fingerprints in the congenitally blind as compared to sighted individuals in order to

6 provide insights into the neuronal mechanisms underlying plasticity in congenital blindness. In

7 the cross-group classification, brain areas of individual congenitally blind participants were

8 classified based on the group-level spectral clusters of the sighted (S-BF). In order to isolate

9 visual deprivation-related effects, the participant groups were well matched in our study (cf.

10 methods section). While in the cross-group classification the classification for the majority of

11 the brain areas was relatively good (i.e., low ranks; Fig. 3A), spectra related to sensory (auditory

12 and visual), right-frontal, left middle temporal pole and bilateral parts of the cingulate cortex

13 were classified significantly worse as compared to the within-sighted classification (Table 1;

14 Fig. 3B). These findings suggest that spectral properties may have been systematically altered

15 by visual deprivation-related plasticity for certain brain areas. Previously, a non-monotonic re-

16 lationship between plasticity and stability across the cortex has been reported using fMRI (Haak

17 and Beckmann 2019), whereas the plasticity observed in neuronal activity has been related to

18 gene expressions (Ortiz-Terán et al. 2017). Specifically, plasticity likely decreases from early

19 visual to mid-level cortex, but increases again further in the visual cortical hierarchy (Haak and

20 Beckmann 2019).

21 **Spectral Plasticity in Sensory Areas**

22 Altered spectral profiles in the congenitally blind individuals reflect changes in intrinsic brain

23 rhythms and might be linked to cognitive processes. Our findings highlight changes in spectral

24 properties of the auditory and visual cortices due to visual deprivation-related neuroplasticity.

The findings confirm previous reports demonstrating both cross-modal reorganization in visual cortex (Burton 2003; Pascual-Leone et al. 2005; Bedny et al. 2011; Voss and Zatorre 2012; Gudi-Mindermann et al. 2018; Rimmele et al. 2019) and intra-modal reorganization in auditory cortex (Roeder and Neville 2003) in blind humans. Importantly, our findings extend these results by providing evidence for genuine changes in the processing mode of these regions, as indicated by changes in the spectral characteristics, which contribute to a more mechanistic understanding.

Visual brain areas classified as spectrally different between the sighted and the congenitally blind individuals (in both the normalized and non-normalized control analysis) comprised right primary visual cortex (calcarine sulcus) and cuneus (Table 1). In these areas, we observed in the sighted two alpha-band clusters indicating distinct alpha brain rhythms. The posterior alpha rhythm, which is typically observed in visual areas during resting state, likely reflects a mechanism of rhythmic inhibition of task-irrelevant neuronal circuits (Haegens et al. 2011). In our data, we observed one cluster with a clear visual alpha peak at ~10 Hz and a smaller peak in the beta-band (~20 Hz). A second alpha cluster was characterized by a smaller amplitude (note that the two clusters are displayed by two separate lines in Fig. 4A), corroborating previous work suggesting distinct visual alpha rhythms (Barzegaran et al. 2017). In contrast, in the congenitally blind individuals these typical visual areas were characterized by a first cluster with a peak at higher frequencies (low gamma, ~40 Hz) and a strongly reduced alpha power peak, as well as a second cluster with low power in the alpha band (Fig. 4A, 4B). This observation is in line with previous findings reporting a reduced or entirely absent alpha rhythm in the visual system in blind individuals (Adrian and Matthews 1934; Noebels et al. 1978; Kriegseis et al. 2006; Hawellek et al. 2013). The reduced alpha brain rhythm is thought to reflect atrophy or reorganization of the cortico-thalamic and cortical pathways, where posterior alpha generators have been located (Lopes da Silva 1991; Lőrincz et al. 2009). It has been proposed that synchronized

posterior gamma activity is controlled by alpha (de-)synchronization and that it indicates increased neuronal gain allowing feedforward processing of sensory information (van Kerkoerle et al. 2014; Michalareas et al. 2016). The gamma rhythm in sighted individuals is typically increased in the presence of a visual stimulus, but decreased or absent during rest. The gamma rhythm may be preserved in blind individuals, as it evidently emerges locally in the occipital cortex (Bastos et al. 2014; Marshall et al. 2018) being less impacted by atrophy of the thalamo-cortical pathway. The presence of gamma activity in blind individuals during rest possibly reflects the alteration of the alpha-gamma excitation-inhibition balance, i.e., the reduced alpha rhythm may result in a disinhibition of visual cortex increasing gamma band activity (Roeder et al.). Functionally, while the reduced alpha rhythm in the congenitally blind may reflect cortical and thalamo-cortical atrophy, the gamma-band rhythm might be related to the compensatory reorganization of visual cortex, i.e., the recruitment of visual cortex during the processing of non-visual tasks (Voss and Zatorre 2012; Striem-Amit et al. 2015; Bedny 2017; Voss 2019). This conjecture is in line with our correlation analysis of the spectral profiles with microstructural white matter properties (Fig. S4, Table S1), which showed that only the alpha cluster correlated with the deteriorated white matter properties.

Additionally, we found altered spectral profiles in right auditory cortex (Heschl's gyrus; Table 1) with increases in power in specific frequency bands. In this area, we observed increased power in the theta-to-beta frequencies in blind as compared to sighted participants (Fig. 4A, 4B). Importantly, in a comparison of auditory cortex spectral profiles during rest and during speech comprehension, Keitel and Gross (2016) provided evidence for the functional relevance of intrinsic delta, theta and beta brain rhythms, as observed during rest, for speech processing. Speech tracking in the theta band (i.e., the phase-locking of auditory cortex oscillatory activity to speech acoustics) is tightly linked to the temporal segmentation of syllables, as well as to the prediction of upcoming stimuli (Giraud and Poeppel 2012; Gross et al. 2013; Haegens and Zion

1   Golumbic 2018; Rimmele, Gross, et al. 2018; Rimmele, Morillon, et al. 2018). Moreover, these

2   auditory cortex brain rhythms seem crucial for the segmentation of sound and music (Doelling

3   and Poeppel 2015; Morillon and Baillet 2017). Interestingly, previous research has shown that

4   congenitally blind individuals are able to comprehend ultra-fast speech at rates where speech

5   comprehension fails in sighted individuals (i.e., speech comprehension in sighted individuals

6   has been shown to fail at syllable rates faster than the theta range; Brungart et al. 2007; Ghitza

7   and Greenberg 2009). Furthermore, this ability to process ultra-fast speech in the congenitally

8   blind individuals has been linked to accelerated theta brain rhythms in right auditory cortex

9   (Hertrich et al. 2013) (see also: Trouvain 2007; Hertrich et al. 2009; Dietrich et al. 2013; Van

10 Ackeren et al. 2018). A possibility is that the altered spectral profiles in congenitally blind in-

11 dividuals reflect intrinsic brain rhythms that aid auditory temporal segmentation skills. Future

12 research, however, is required to confirm this speculation by relating the changes in brain

13 rhythms to behavioral performance.

14 **Spectral Plasticity Beyond Sensory Cortices**

15 Beyond spectral reorganization in sensory cortices, our data suggest that also right-hemispheric

16 frontal brain regions, bilateral parts of the cingulate cortex (left anterior, and right middle) and

17 the left middle temporal pole undergo adaptation. Spectral clusters of right medial superior

18 frontal gyrus and cingulate cortices were classified as different between the blind and the

19 sighted groups, with increased power in the theta-band in the blind group. Medial superior

20 frontal gyrus has been linked to various cognitive processes (Cohen et al. 2009; Cavanagh and

21 Frank 2014; Chander et al. 2016; Töllner et al. 2017), as well as theta-band brain rhythms (Ku-

22 bota et al. 2001; Onton et al. 2005; Cohen et al. 2008; Cohen 2011; Itthipuripat et al. 2013;

23 Hsieh and Ranganath 2014; Töllner et al. 2017; Eschmann et al. 2018; Başar-Eroglu et al.). For

24 instance, medial superior frontal gyrus has been implicated in cognitive control (Cavanagh and

25 Frank 2014), cognitive control of timing (Lewis and Miall 2003), decision making (Schmidt et

al. 2018), working memory (Itthipuripat et al. 2013; Hsieh and Ranganath 2014), temporal order processing (Chander et al. 2016), or language processing (Binder et al. 2009). Some of these processes are presumably altered in congenital blind individuals as compared to sighted individuals, such as language processing in a frontotemporal network (Roeder et al. 2002; Lane et al. 2017), and temporal order processing (Roeder et al. 2004; Stevens and Weaver 2005).

The cingulate cortex (among other processes) has been associated with emotion, cognitive control and pain processing (Shackman et al. 2011). The left temporal pole, part of the anterior temporal lobe, is thought to be involved in various processes including semantic (Binder et al. 1999; Visser and Lambon Ralph 2011) and conceptual (Baron and Osherson 2011) processing. For both the cingular (Ortiz-Terán et al. 2016) and anterior temporal (Striem-Amit et al. 2018) structures altered brain responses have been observed and proposed to be related to adaptive behavior in congenitally blind as compared to sighted individuals. However, as the functionality of these structures in congenital blindness, and particularly the role of endogenous brain rhythms, remain little understood, we refrain from further interpreting these findings.

Note, that for some brain areas we found differences in spectral profiles in the cross-group classification analysis (normalized data), however, not in the control analysis (on the non-normalized data; Table 1; Fig. 3C, Table S2). We applied a previously established (Keitel & Gross, 2016) procedure. A disadvantage of the procedure is that it might introduce spurious activity due to group differences in the normalization spectrum, as the procedure normalizes the spectra across the brain. An advantage of the procedure is that it down-weights the neuronal activity (1/f power) that is predominant across the brain and not specific to a given brain area, which otherwise complicates the spectral analysis. Thus, without the normalization the noise-level of the data is increased due to individual differences in overall power across the spectrum and across the brain. Although these arguments justify our choice, as precautionary measure we only interpreted effects found in both analyses.

Spectral profiles related to microstructural white matter properties

A relevant question is to what extent our findings of altered spectral profiles of occipital cortex in the congenitally blind are linked to structural differences. Our DTI analysis revealed compromised white matter integrity in congenitally blind individuals in visual association tracts comprising the ventral visual stream. These tracts included the bilateral inferior fronto-occipital fasciculus, connecting occipital and frontal brain areas and the bilateral inferior longitudinal fasciculus, connecting occipital and anterior temporal cortices, which have been conjectured to play a role in reading, writing and language semantics (Catani and Mesulam 2008); and the bilateral optic radiations, linking the visual thalamus to the primary visual cortex. In addition, white matter integrity was also compromised in the posterior corpus callosum, by which homologous visual cortices are interconnected (Restani and Caleo 2016). Reduced white matter integrity in early (Shimony et al. 2006; Park et al. 2007), late (Wang et al. 2013; Hofstetter et al. 2019), and congenitally blind individuals (Ptito et al. 2008; Wang et al. 2013; Aguirre et al. 2016; Reislev et al. 2016), particularly in visual pathways (e.g., optic radiations and the corpus callosum), is a well-documented finding. As myelination is proportional to the degree of neuronal activation during brain development (Demerens et al. 1996; Stevens et al. 2002; Fields 2004; Ishibashi et al. 2006; Gautier et al. 2015; Wake et al. 2015), the lack of visual processing during development in congenital blindness likely causes the reduced white matter density in visual pathways (Hill et al. 2014; Dietz et al. 2016; Restani and Caleo 2016; Anurova et al. 2019). Our findings show that reduced spectral power in the visual alpha rhythm co-occurred with reduced white matter integrity in pathways that overlap with visual cortical pathways and thalamo-cortical projections (i.e., negative correlation between alpha power and RD; Fig. S4B), confirming previous accounts suggesting that reduced visual alpha power originates in structural impairment (Adrian and Matthews 1934; Noebels et al. 1978; Kriegseis et al. 2006; Hawellek et al. 2013).

Concluding Remarks

The present study supports the findings of robust brain area-specific spectral profiles in the human brain. We provide, for the first time, a whole-brain model of spectral fingerprints in congenitally blind adults, and crucially, we were able to map spectral changes due to visual deprivation to specific—namely right visual, auditory, frontal, left anterior temporal, and bilateral cingulate—brain areas. We suggest that the power increases in the theta-to-beta frequency bands in auditory and frontal brain regions may reflect adaptive sensory or higher cognitive processing in blind individuals, while altered spectral profiles in visual brain regions (lower alpha and a gamma peak) may indicate a change in the excitation-inhibition balance. While these interpretations are tentative, the results pave the way for more targeted, task-based studies that aim to identify the link between altered spectral profiles and adaptive behavior.

Competing Interests

The authors declare that no competing interests exist.

References

Adrian ED, Matthews BH. 1934. The Berger rhythm: potential changes from the occipital lobes in man. Brain. 57(4):355–385.

Aguirre GK, Datta R, Benson NC, Prasad S, Jacobson SG, Cideciyan AV, Bridge H, Watkins KE, Butt OH, Dain AS, et al. 2016. Patterns of individual variation in visual pathway structure and function in the sighted and blind. PLOS ONE. 11(11):e0164677. doi:10.1371/journal.pone.0164677.

Amedi A, Raz N, Pianka P, Malach R, Zohary E. 2003. Early 'visual' cortex activation correlates with superior verbal memory performance in the blind. Nat Neurosci. 6(7):758–766. doi:10.1038/nn1072.

Andersson JLR, Jenkinson M, Smith S. 2007. Non-linear registration, aka spatial normalisation. FMRIB Technial Report TR07JA2. (Oxford Centre for Functional Magnetic Resonance Imaging of the Brain, Department of Clinical Neurology, Oxford University). 62.

Anurova I, Carlson S, Rauschecker JP. 2019. Overlapping Anatomical Networks Convey Cross-Modal Suppression in the Sighted and Coactivation of "Visual" and Auditory Cortex in the Blind. Cereb Cortex. 29(11):4863–4876. doi:10.1093/cercor/bhz021.

Arnal LH, Doelling KB, Poeppel D. 2015. Delta–beta coupled oscillations underlie temporal prediction accuracy. Cereb Cortex. 25(9):3077–3085. doi:10.1093/cercor/bhu103.

Aung WY, Mar S, Benzinger TL. 2013. Diffusion tensor MRI as a biomarker in axonal and myelin damage. Imaging Med. 5(5):427–440. doi:10.2217/iim.13.49.

Baron SG, Osherson D. 2011. Evidence for conceptual combination in the left anterior temporal lobe. NeuroImage. 55(4):1847–1852. doi:10.1016/j.neuroimage.2011.01.066.

1 Barzegaran E, Vildavski VY, Knyazeva MG. 2017. Fine structure of posterior alpha rhythm in

2   human EEG: Frequency components, their cortical sources, and temporal behavior. Sci

3   Rep. 7(1):8249. doi:10.1038/s41598-017-08421-z.

4 Başar-Eroglu C, Başar E, Demiralp T, Schürmann M. P300-response: possible psychophysio-

5   logical correlates in delta and theta frequency channels. A review. Int J Psychophysiol.

6   13(2):161–179.

7 Bastos AM, Briggs F, Alitto HJ, Mangun GR, Usrey WM. 2014. Simultaneous recordings from

8   the primary visual cortex and lateral geniculate nucleus reveal rhythmic interactions and a

9   cortical   source   for   gamma-band   oscillations.   J   Neurosci.   34(22):7639–7644.

10   doi:10.1523/JNEUROSCI.4216-13.2014.

11 Bedny M. 2017. Evidence from blindness for a cognitively pluripotent cortex. Trends Cogn Sci.

12   21(9):637–648. doi:10.1016/j.tics.2017.06.003.

13 Bedny M, Pascual-Leone A, Dodell-Feder D, Fedorenko E, Saxe R. 2011. Language processing

14   in the occipital cortex of congenitally blind adults. Proc Natl Acad Sci. 108(11):4429–4434.

15   doi:10.1073/pnas.1014818108.

16 Binder JR, Desai RH, Graves WW, Conant LL. 2009. Where Is the semantic system? A critical

17   review   and   meta-analysis   of   120   functional   neuroimaging   studies.   Cereb   Cortex.

18   19(12):2767–2796. doi:10.1093/cercor/bhp055.

19 Binder JR, Frost JA, Hammeke TA, Bellgowan PSF, Rao SM, Cox RW. 1999. Conceptual

20   Processing during the Conscious Resting State: A Functional MRI Study. J Cogn Neurosci.

21   11(1):80–93. doi:10.1162/089892999563265.

22 Brookes MJ, Woolrich M, Luckhoo H, Price D, Hale JR, Stephenson MC, Barnes GR, Smith

23   SM, Morris PG. 2011. Investigating the electrophysiological basis of resting state networks

using magnetoencephalography. Proc Natl Acad Sci. 108(40):16783–16788. doi:10.1073/pnas.1112685108.

Brungart DS, van Wassenhove V, Brandewie E, Romigh G. 2007. The effects of temporal acceleration and deceleration on AV speech perception. AVSP.:27–34.

Buffalo EA, Fries P, Landman R, Buschman TJ, Desimone R. 2011. Laminar differences in gamma and alpha coherence in the ventral stream. Proc Natl Acad Sci. 108(27):11262–11267. doi:10.1073/pnas.1011284108.

Bull R, Rathborn H, Clifford BR. 1983. The voice-recognition accuracy of blind listeners. Perception. 12(2):223–226. doi:10.1068/p120223.

Burton H. 2003. Visual cortex activity in early and late blind people. J Neurosci. 23(10):4005–4011. doi:10.1523/JNEUROSCI.23-10-04005.2003.

Buzsáki G. 2004. Neuronal oscillations in cortical networks. Science. 304(5679):1926–1929. doi:10.1126/science.1099745.

Buzsáki G, Logothetis N, Singer W. 2013. Scaling brain size, keeping timing: evolutionary preservation of brain rhythms. Neuron. 80(3):751–764. doi:10.1016/j.neuron.2013.10.002.

Carrara-Augustenborg C, Schultz BG. 2019. The implicit learning of metrical and non-metrical rhythms in blind and sighted adults. Psychol Res. 83(5):907–923. doi:10.1007/s00426-017-0916-0.

Catani M, Mesulam M. 2008. The arcuate fasciculus and the disconnection theme in language and aphasia: History and current state. Cortex. 44(8):953–961. doi:10.1016/j.cortex.2008.04.002.

Cavanagh JF, Frank MJ. 2014. Frontal theta as a mechanism for cognitive control. Trends Cogn Sci. 18(8):414–421. doi:10.1016/j.tics.2014.04.012.

Chander BS, Witkowski M, Braun C, Robinson SE, Born J, Cohen LG, Birbaumer N, Soekadar SR. 2016. tACS Phase Locking of Frontal Midline Theta Oscillations Disrupts Working Memory Performance. Front Cell Neurosci. 10. doi:10.3389/fncel.2016.00120. http://journal.frontiersin.org/Article/10.3389/fncel.2016.00120/abstract.

Cohen MX. 2011. Error-related medial frontal theta activity predicts cingulate-related structural connectivity. NeuroImage. 55(3):1373–1383. doi:10.1016/j.neuroimage.2010.12.072.

Cohen MX, Elger CE, Fell J. 2009. Oscillatory activity and phase–amplitude coupling in the human medial frontal cortex during decision making. J Cogn Neurosci. 21(2):390–402. doi:10.1162/jocn.2008.21020.

Cohen MX, Ridderinkhof KR, Haupt S, Elger CE, Fell J. 2008. Medial frontal cortex and response conflict: Evidence from human intracranial EEG and medial frontal cortex lesion. Brain Res. 1238:127–142. doi:10.1016/j.brainres.2008.07.114.

Deco G, Jirsa VK, McIntosh AR. 2011. Emerging concepts for the dynamical organization of resting-state activity in the brain. Nat Rev Neurosci. 12(1):43–56. doi:10.1038/nrn2961.

Demerens C, Stankoff B, Logak M, Anglade P, Allinquant B, Couraud F, Zalc B, Lubetzki C. 1996. Induction of myelination in the central nervous system by electrical activity. Proc Natl Acad Sci. 93(18):9887–9892. doi:10.1073/pnas.93.18.9887.

Dietrich S, Hertrich I, Ackermann H. 2013. Ultra-fast speech comprehension in blind subjects engages primary visual cortex, fusiform gyrus, and pulvinar – a functional magnetic resonance imaging (fMRI) study. BMC Neurosci. 14(1). doi:10.1186/1471-2202-14-74.

Dietz KC, Polanco JJ, Pol SU, Sim FJ. 2016. Targeting human oligodendrocyte progenitors for myelin repair. Exp Neurol. 283:489–500. doi:10.1016/j.expneurol.2016.03.017.

Doelling KB, Arnal LH, Ghitza O, Poeppel D. 2014. Acoustic landmarks drive delta–theta oscillations to enable speech comprehension by facilitating perceptual parsing. NeuroImage. 85:761–768. doi:10.1016/j.neuroimage.2013.06.035.

Doelling KB, Poeppel D. 2015. Cortical entrainment to music and its modulation by expertise. Proc Natl Acad Sci. 112(45):E6233–E6242. doi:10.1073/pnas.1508431112.

Elbert T, Sterr A, Rockstroh B, Pantev C, Müller MM, Taub E. 2002. Expansion of the tonotopic area in the auditory cortex of the blind. J Neurosci. 22(22):9941–9944. doi:10.1523/JNEUROSCI.22-22-09941.2002.

Engel AK, Fries P, Singer W. 2001. Dynamic predictions: Oscillations and synchrony in top–down processing. Nat Rev Neurosci. 2(10):704–716. doi:10.1038/35094565.

Engel AK, Gerloff C, Hilgetag CC, Nolte G. 2013. Intrinsic coupling modes: Multiscale interactions in ongoing brain activity. Neuron. 80(4):867–886. doi:10.1016/j.neuron.2013.09.038.

Engel AK, König P, Kreiter AK, Schillen TB, Singer W. 1992. Temporal coding in the visual cortex: new vistas on integration in the nervous system. Trends Neurosci. 15(6):218–226. doi:10.1016/0166-2236(92)90039-B.

Eschmann KCJ, Bader R, Mecklinger A. 2018. Topographical differences of frontal-midline theta activity reflect functional differences in cognitive control abilities. Brain Cogn. 123:57–64. doi:10.1016/j.bandc.2018.02.002.

Ferrarelli F, Sarasso S, Guller Y, Riedner BA, Peterson MJ, Bellesi M, Massimini M, Postle BR, Tononi G. 2012. Reduced natural oscillatory frequency of frontal thalamocortical circuits in schizophrenia. Arch Gen Psychiatry. 69(8). doi:10.1001/archgenpsychiatry.2012.147.

Fields RD. 2004. Volume transmission in activity-dependent regulation of myelinating glia. Neurochem Int. 45(4):503–509. doi:10.1016/j.neuint.2003.11.015.

Foecker J, Best A, Hoelig C, Roeder B. 2012. The superiority in voice processing of the blind arises from neural plasticity at sensory processing stages. Neuropsychologia. 50(8):2056–2067. doi:10.1016/j.neuropsychologia.2012.05.006.

Fujioka T, Trainor LJ, Large EW, Ross B. 2012. Internalized Timing of Isochronous Sounds Is Represented in Neuromagnetic Beta Oscillations. J Neurosci. 32(5):1791–1802. doi:10.1523/JNEUROSCI.4107-11.2012.

Gautier HOB, Evans KA, Volbracht K, James R, Sitnikov S, Lundgaard I, James F, Lao-Peregrin C, Reynolds R, Franklin RJM, et al. 2015. Neuronal activity regulates remyelination via glutamate signalling to oligodendrocyte progenitors. Nat Commun. 6(1):8518. doi:10.1038/ncomms9518.

Ghitza O, Greenberg S. 2009. On the possible role of brain rhythms in speech perception: Intelligibility of time-compressed speech with periodic and aperiodic insertions of silence. Phonetica. 66(1–2):113–126. doi:10.1159/000208934.

Giraud A-L, Kleinschmidt A, Poeppel D, Lund TE, Frackowiak RSJ, Laufs H. 2007. Endogenous cortical rhythms determine cerebral specialization for speech perception and production. Neuron. 56(6):1127–1134. doi:10.1016/j.neuron.2007.09.038.

Giraud A-L, Poeppel D. 2012. Cortical oscillations and speech processing: emerging computational principles and operations. Nat Neurosci. 15(4):511–517. doi:10.1038/nn.3063.

Gougoux F, Belin P, Voss P, Lepore F, Lassonde M, Zatorre RJ. 2009. Voice perception in blind persons: A functional magnetic resonance imaging study. Neuropsychologia. 47(13):2967–2974. doi:10.1016/j.neuropsychologia.2009.06.027.

Gougoux F, Lepore F, Lassonde M, Voss P, Zatorre RJ, Belin P. 2004. Pitch discrimination in the early blind. Nature. 430(6997):309–309. doi:10.1038/430309a.

Gougoux F, Zatorre RJ, Lassonde M, Voss P, Lepore F. 2005. A functional neuroimaging study of sound localization: visual cortex activity predicts performance in early-blind individuals. Raichle M, editor. PLoS Biol. 3(2):e27. doi:10.1371/journal.pbio.0030027.

Gross J, Hoogenboom N, Thut G, Schyns P, Panzeri S, Belin P, Garrod S. 2013. Speech rhythms and multiplexed oscillatory sensory coding in the human brain. Poeppel D, editor. PLoS Biol. 11(12):e1001752. doi:10.1371/journal.pbio.1001752.

Gudi-Mindermann H, Rimmele JM, Nolte G, Bruns P, Engel AK, Roeder B. 2018. Working memory training in congenitally blind individuals results in an integration of occipital cortex in functional networks. Behav Brain Res. 348:31–41. doi:10.1016/j.bbr.2018.04.002.

Haak K, Beckmann CF. 2019. Plasticity versus stability across the human cortical visual connectome. bioRxiv. doi:10.1101/520395.

Haegens S, Nacher V, Luna R, Romo R, Jensen O. 2011. Alpha-Oscillations in the monkey sensorimotor network influence discrimination performance by rhythmical inhibition of neuronal spiking. Proc Natl Acad Sci. 108(48):19377–19382. doi:10.1073/pnas.1117190108.

Haegens S, Zion Golumbic E. 2018. Rhythmic facilitation of sensory processing: A critical review. Neurosci Biobehav Rev. 86:150–165. doi:10.1016/j.neubiorev.2017.12.002.

Hawellek DJ, Schepers IM, Roeder B, Engel AK, Siegel M, Hipp JF. 2013. Altered intrinsic neuronal interactions in the visual cortex of the blind. J Neurosci. 33(43):17072–17080. doi:10.1523/JNEUROSCI.1625-13.2013.

1   Henry MJ, Herrmann B, Obleser J. 2014. Entrained neural oscillations in multiple frequency

2   bands comodulate behavior. Proc Natl Acad Sci. 111(41):14935–14940.

3   doi:10.1073/pnas.1408741111.

4   Hertrich I, Dietrich S, Ackermann H. 2013. Tracking the speech signal – Time-locked MEG

5   signals during perception of ultra-fast and moderately fast speech in blind and in sighted

6   listeners. Brain Lang. 124(1):9–21. doi:10.1016/j.bandl.2012.10.006.

7   Hertrich I, Dietrich S, Moos A, Trouvain J, Ackermann H. 2009. Enhanced speech perception

8   capabilities in a blind listener are associated with activation of fusiform gyrus and primary

9   visual cortex. Neurocase. 15(2):163–170. doi:10.1080/13554790802709054.

10   Heusser AC, Poeppel D, Ezzyat Y, Davachi L. 2016. Episodic sequence memory is supported

11   by a theta–gamma phase code. Nat Neurosci. 19(10):1374–1380. doi:10.1038/nn.4374.

12   Hill RA, Patel KD, Goncalves CM, Grutzendler J, Nishiyama A. 2014. Modulation of oligoden-

13   drocyte generation during a critical temporal window after NG2 cell division. Nat Neurosci.

14   17(11):1518–1527. doi:10.1038/nn.3815.

15   Hipp JF, Engel AK, Siegel M. 2011. Oscillatory synchronization in large-scale cortical net-

16   works predicts perception. Neuron. 69(2):387–396. doi:10.1016/j.neuron.2010.12.027.

17   Hipp JF, Hawellek DJ, Corbetta M, Siegel M, Engel AK. 2012. Large-scale cortical correlation

18   structure of spontaneous oscillatory activity. Nat Neurosci. 15(6):884–890.

19   doi:10.1038/nn.3101.

20   Hoetting K, Roesler F, Roeder B. 2004. Altered auditory-tactile interactions in congenitllally

21   blind humans: an event-related potential study. Exp Brain Res. 159:370–381. doi:DOI

22   10.1007/s00221-004-1965-3.

1 Hofstetter S, Sabbah N, Mohand-Saïd S, Sahel J-A, Habas C, Safran AB, Amedi A. 2019. The

2   development of white matter structural changes during the process of deterioration of the

3   visual field. Sci Rep. 9(1):2085. doi:10.1038/s41598-018-38430-5.

4 Holcombe AO. 2009. Seeing slow and seeing fast: two limits on perception. Trends Cogn Sci.

5   13(5):216–221. doi:10.1016/j.tics.2009.02.005.

6 Hsieh L-T, Ranganath C. 2014. Frontal midline theta oscillations during working memory

7   maintenance and episodic encoding and retrieval. NeuroImage. 85:721–729.

8   doi:10.1016/j.neuroimage.2013.08.003.

9 Ishibashi T, Dakin KA, Stevens B, Lee PR, Kozlov SV, Stewart CL, Fields RD. 2006. Astro-

10   cytes promote myelination in response to electrical impulses. Neuron. 49(6):823–832.

11   doi:10.1016/j.neuron.2006.02.006.

12 Itthipuripat S, Wessel JR, Aron AR. 2013. Frontal theta is a signature of successful working

13   memory manipulation. Exp Brain Res. 224(2):255–262. doi:10.1007/s00221-012-3305-3.

14 Jenkinson M, Beckmann CF, Behrens TEJ, Woolrich MW, Smith SM. 2012. FSL. NeuroImage.

15   62(2):782–790. doi:10.1016/j.neuroimage.2011.09.015.

16 Jensen O, Bonnefond M, VanRullen R. 2012. An oscillatory mechanism for prioritizing salient

17   unattended stimuli. Trends Cogn Sci. 16(4):200–206. doi:10.1016/j.tics.2012.03.002.

18 Jensen O, Mazaheri A. 2010. Shaping functional architecture by oscillatory alpha activity: Gat-

19   ing by inhibition. Front Hum Neurosci. 4. doi:10.3389/fnhum.2010.00186.

20 Keitel A, Gross J. 2016. Individual human brain areas can be identified from their characteristic

21   spectral activation fingerprints. Engel AK, editor. PLOS Biol. 14(6):e1002498.

22   doi:10.1371/journal.pbio.1002498.

van Kerkoerle T, Self MW, Dagnino B, Gariel-Mathis M-A, Poort J, van der Togt C, Roelfsema PR. 2014. Alpha and gamma oscillations characterize feedback and feedforward processing in monkey visual cortex. Proc Natl Acad Sci. 111(40):14332–14341. doi:10.1073/pnas.1402773111.

Klawiter EC, Schmidt RE, Trinkaus K, Liang H-F, Budde MD, Naismith RT, Song S-K, Cross AH, Benzinger TL. 2011. Radial diffusivity predicts demyelination in ex vivo multiple sclerosis spinal cords. NeuroImage. 55(4):1454–1460. doi:10.1016/j.neuroimage.2011.01.007.

Klimesch W, Sauseng P, Hanslmayr S. 2007. EEG alpha oscillations: The inhibition–timing hypothesis. Brain Res Rev. 53(1):63–88. doi:10.1016/j.brainresrev.2006.06.003.

Korte M, Rauschecker JP. 1993. Auditory spatial tuning of cortical neurons is sharpened in cats with early blindness. J Neurophysiol. 70(4):1717–1721. doi:10.1152/jn.1993.70.4.1717.

Kriegseis A, Hennighausen E, Roesler F, Roeder B. 2006. Reduced EEG alpha activity over parieto-occipital brain areas in congenitally blind adults. Clin Neurophysiol. 117(7):1560–1573. doi:10.1016/j.clinph.2006.03.030.

Kubota Y, Sato W, Toichi M, Murai T, Okada T, Hayashi A, Sengoku A. 2001. Frontal midline theta rhythm is correlated with cardiac autonomic activities during the performance of an attention demanding meditation procedure. Cogn Brain Res. 11(2):281–287. doi:10.1016/S0926-6410(00)00086-0.

Lakatos P, Karmos G, Mehta AD, Ulbert I, Schroeder CE. 2008. Entrainment of neuronal os-cillations as a mechanism of attentional selection. Science. 320(5872):110–113. doi:10.1126/science.1154735.

Lakatos P, Musacchia G, O'Connel MN, Falchier AY, Javitt DC, Schroeder CE. 2013. The spectrotemporal flter mechanism of auditory selective attention. Neuron. 77(4):750–761. doi:10.1016/j.neuron.2012.11.034.

Lakatos P, Shah AS, Knuth KH, Ulbert I, Karmos G, Schroeder CE. 2005. An oscillatory hierarchy controlling neuronal excitability and stimulus processing in the auditory cortex. J Neurophysiol. 94(3):1904–1911. doi:10.1152/jn.00263.2005.

Lane C, Kanjlia S, Richardson H, Fulton A, Omaki A, Bedny M. 2017. Reduced left lateralization of language in congenitally blind individuals. J Cogn Neurosci. 29(1):65–78. doi:10.1162/jocn_a_01045.

Lerens E, Araneda R, Renier L, De Volder AG. 2014. Improved beat asynchrony detection in early blind individuals. Perception. 43(10):1083–1096. doi:10.1068/p7789.

Lessard N, Paré M, Lepore F, Lassonde M. 1998. Early-blind human subjects localize sound sources better than sighted subjects. Nature. 395(6699):278–280. doi:10.1038/26228.

Lewis PA, Miall RC. 2003. Distinct systems for automatic and cognitively controlled time measurement: evidence from neuroimaging. Curr Opin Neurobiol. 13(2):250–255. doi:10.1016/S0959-4388(03)00036-9.

Lopes da Silva F. 1991. Neural mechanisms underlying brain waves: from neural membranes to networks. Electroencephalogr Clin Neurophysiol. 79(2):81–93. doi:10.1016/0013-4694(91)90044-5.

Lőrincz ML, Kékesi KA, Juhász G, Crunelli V, Hughes SW. 2009. Temporal framing of thalamic relay-mode firing by phasic inhibition during the alpha rhythm. Neuron. 63(5):683–696. doi:10.1016/j.neuron.2009.08.012.

Luo H, Poeppel D. 2007. Phase patterns of neuronal responses reliably discriminate speech in human auditory cortex. Neuron. 54(6):1001–1010. doi:10.1016/j.neuron.2007.06.004.

MacQueen J. 1967. Some methods for classification and analysis of multivariate observations. Proc Fifth Berkeley Symp Math Stat Probab. 1(14):281–297.

Marshall TR, den Boer S, Cools R, Jensen O, Fallon SJ, Zumer JM. 2018. Occipital alpha and gamma oscillations support complementary mechanisms for processing stimulus value associations. J Cogn Neurosci. 30(1):119–129. doi:10.1162/jocn_a_01185.

Michalareas G, Vezoli J, van Pelt S, Schoffelen J-M, Kennedy H, Fries P. 2016. Alpha-beta and gamma rhythms subserve feedback and feedforward influences among human visual cortical areas. Neuron. 89(2):384–397. doi:10.1016/j.neuron.2015.12.018.

Moos A, Trouvain J. 2007. Comprehension of ultra-fast speech - blind vs. "normally-hearing" persons. Proc 16th Int Congr Phon Sci. 1:677–680.

Morillon B, Baillet S. 2017. Motor origin of temporal predictions in auditory attention. Proc Natl Acad Sci. 114(42):E8913–E8921. doi:10.1073/pnas.1705373114.

Nichols TE, Holmes AP. 2002. Nonparametric permutation tests for functional neuroimaging: A primer with examples. Hum Brain Mapp. 15(1):1–25. doi:10.1002/hbm.1058.

Noebels JL, Roth WT, Kopell BS. 1978. Cortical slow potentials and the occipital EEG in congenital blindness. J Neurol Sci. 37(1–2):51–58. doi:10.1016/0022-510X(78)90227-7.

Noppeney U. 2007. The effects of visual deprivation on functional and structural organization of the human brain. Neurosci Biobehav Rev. 31(8):1169–1180. doi:10.1016/j.neubiorev.2007.04.012.

Noppeney U, Friston KJ, Ashburner J, Frackowiak R, Price CJ. 2005. Early visual deprivation induces structural plasticity in gray and white matter. Curr Biol. 15(13):R488–R490. doi:10.1016/j.cub.2005.06.053.

Onton J, Delorme A, Makeig S. 2005. Frontal midline EEG dynamics during working memory. NeuroImage. 27(2):341–356. doi:10.1016/j.neuroimage.2005.04.014.

Ortiz-Terán L, Ortiz T, Perez DL, Aragón JI, Diez I, Pascual-Leone A, Sepulcre J. 2016. Brain Plasticity in Blind Subjects Centralizes Beyond the Modal Cortices. Front Syst Neurosci. 10. doi:10.3389/fnsys.2016.00061.

Park H-J, Jeong S-O, Kim EY, Kim D-J, Kim SY, Lee SC, Lee JD. 2007. Reorganization of neural circuits in the blind on di¡usion direction analysis. :4.

Pascual-Leone A, Amedi A, Fregni F, Merabet LB. 2005. The plastic human brain cortex. Annu Rev Neurosci. 28(1):377–401. doi:10.1146/annurev.neuro.27.070203.144216.

Pascual-Leone A, Torres F. 1993. Plasticity of the sensorimotor cortex representation of the reading finger in Braille readers. Brain. 116(1):39–52. doi:10.1093/brain/116.1.39.

de Pasquale F, Della Penna S, Snyder AZ, Lewis C, Mantini D, Marzetti L, Belardinelli P, Ciancetta L, Pizzella V, Romani GL, et al. 2010. Temporal dynamics of spontaneous MEG activity in brain networks. Proc Natl Acad Sci. 107(13):6040–6045. doi:10.1073/pnas.0913863107.

Pittman-Polletta BR, Wang Y, Stanley DA, Schroeder CE, Whittington MA, Kopell NJ. 2020. Differential contributions of synaptic and intrinsic inhibitory currents to speech segmentation via flexible phase-locking in neural oscillators. bioRxiv. doi:10.1101/2020.01.11.902858.

Portoles O, Borst JP, van Vugt MK. 2018. Characterizing synchrony patterns across cognitive task stages of associative recognition memory. Eur J Neurosci. 48(8):2759–2769. doi:10.1111/ejn.13817.

Ptito M, Schneider FCG, Paulson OB, Kupers R. 2008. Alterations of the visual pathways in congenital blindness. Exp Brain Res. 187(1):41–49. doi:10.1007/s00221-008-1273-4.

Raichle ME. 2011. The restless brain. Brain Connect. 1(1):3–12. doi:10.1089/brain.2011.0019.

Raichle ME. 2015. The restless brain: how intrinsic activity organizes brain function. Philos Trans R Soc B Biol Sci. 370(1668):20140172. doi:10.1098/rstb.2014.0172.

Rauschecker JP. 2008. Plasticity of cortical maps in visual deprivation. In: Blindness and brain plasticity in navigation and object perception. Taylor & Francis. p. 43–66.

Rauschecker JP, Tian B, Korte M, Egert U. 1992. Crossmodal changes in the somatosensory vibrissa/barrel system of visually deprived animals. Proc Natl Acad Sci. 89(11):5063–5067. doi:10.1073/pnas.89.11.5063.

Reislev NL, Dyrby TB, Siebner HR, Kupers R, Ptito M. 2016. Simultaneous assessment of white matter changes in microstructure and connectedness in the blind brain. Neural Plast. 2016:1–12. doi:10.1155/2016/6029241.

Restani L, Caleo M. 2016. Reorganization of visual callosal connections following alterations of retinal input and brain damage. Front Syst Neurosci. 10. doi:10.3389/fnsys.2016.00086.

Reynolds DA, Rose RC. 1995. Robust text-independent speaker identification using Gaussian mixture speaker models. IEEE Trans Speech Audio Process. 3(1):72–83. doi:10.1109/89.365379.

Rimmele JM, Gross J, Molholm S, Keitel A. 2018. Editorial: Brain oscillations in human communication. Front Hum Neurosci. 12. doi:10.3389/fnhum.2018.00039.

Rimmele JM, Gudi-Mindermann H, Nolte G, Roeder B, Engel AK. 2019. Working memory training integrates visual cortex into beta-band networks in congenitally blind individuals. NeuroImage. 194:259–271. doi:10.1016/j.neuroimage.2019.03.003.

Rimmele JM, Morillon B, Poeppel D, Arnal LH. 2018. Proactive sensing of periodic and aperiodic auditory patterns. Trends Cogn Sci. 22(10):870–882. doi:10.1016/j.tics.2018.08.003.

Roeder B, Demuth L, Streb J, Roesler F. 2003. Semantic and morpho-syntactic priming in auditory word recognition in congenitally blind adults. Lang Cogn Process. 18(1):1–20. doi:10.1080/01690960143000407.

Roeder B, Gudi-Mindermann H, Shareef I, Rimmele JM, Sourav S, Kekunnaya R, Bottari D. Spectral profiles of resting state EEG in permanently congenital blind and sight recovery individuals. underRevision.

Roeder B, Kraemer UM, Lange K. 2007. Congenitally blind humans use different stimulus selection strategies in hearing: An ERP study of spatial and temporal attention. Restor Neurol Neurosci. 25(3–4):311–322.

Roeder B, Neville H. 2003. Developmental functional plasticity. Grafman J, Robertson I, editors. Handb Neuropsychol.(9):231–270.

Roeder B, Roesler F, Hennighausen E, Nicker F. 1996. Event-related potentials during auditory and somatosensory discrimination in sighted and blind human subjects. Cogn Brain Res. 4:17.

Roeder B, Roesler F, Neville HJ. 1999. Effects of interstimulus interval on auditory event-related potentials in congenitally blind and normally sighted humans. Neurosci Lett. 264(1–3):53–56. doi:10.1016/S0304-3940(99)00182-2.

Roeder B, Roesler F, Neville HJ. 2000. Event-related potentials during auditory language processing in congenitally blind and sighted people. Neuropsychologia. 38(11):1482–1502. doi:10.1016/S0028-3932(00)00057-9.

Roeder B, Roesler F, Neville HJ. 2001. Auditory memory in congenitally blind adults: A behavioral-electrophysiological investigation. Cogn Brain Res. 11(2):289–303. doi:10.1016/S0926-6410(01)00002-7.

Roeder B, Roesler F, Spence C. 2004. Early vision impairs tactile perception in the blind. Curr Biol. 14(2):121–124. doi:10.1016/j.cub.2003.12.054.

Roeder B, Stock O, Bien S, Neville H, Roesler F. 2002. Speech processing activates visual cortex in congenitally blind humans: Plasticity of language functions in blind adults. Eur J Neurosci. 16(5):930–936. doi:10.1046/j.1460-9568.2002.02147.x.

Rosanova M, Casali A, Bellina V, Resta F, Mariotti M, Massimini M. 2009. Natural Frequencies of Human Corticothalamic Circuits. J Neurosci. 29(24):7679–7685. doi:10.1523/JNEUROSCI.0445-09.2009.

Rousseeuw PJ. 1987. Silhouettes: A graphical aid to the interpretation and validation of cluster analysis. J Comput Appl Math. 20:53–65. doi:10.1016/0377-0427(87)90125-7.

Schepers IM, Hipp JF, Schneider TR, Roeder B, Engel AK. 2012. Functionally specific oscillatory activity correlates between visual and auditory cortex in the blind. Brain. 135(3):922–934. doi:10.1093/brain/aws014.

Schmidt B, Kanis H, Holroyd CB, Miltner WHR, Hewig J. 2018. Anxious gambling: Anxiety is associated with higher frontal midline theta predicting less risky decisions. Psychophysiology. 55(10):e13210. doi:10.1111/psyp.13210.

Schroeder SCY, Ball F, Busch NA. 2018. The role of alpha oscillations in distractor inhibition during memory retention. Eur J Neurosci. 48(7):2516–2526. doi:10.1111/ejn.13852.

Schubert JTW, Buchholz VN, Foecker J, Engel AK, Roeder B, Heed T. 2015. Oscillatory activity reflects differential use of spatial reference frames by sighted and blind individuals in tactile attention. NeuroImage. 117:417–428. doi:10.1016/j.neuroimage.2015.05.068.

Shackman AJ, Salomons TV, Slagter HA, Fox AS, Winter JJ, Davidson RJ. 2011. The integration of negative affect, pain and cognitive control in the cingulate cortex. Nat Rev Neurosci. 12(3):154–167. doi:10.1038/nrn2994.

1 Shimony JS, Burton H, Epstein AA, McLaren DG, Sun SW, Snyder AZ. 2006. Diffusion Ten-

2   sor Imaging Reveals White Matter Reorganization in Early Blind Humans. Cereb Cortex.

3   16(11):1653–1661. doi:10.1093/cercor/bhj102.

4 Siegel M, Donner TH, Engel AK. 2012. Spectral fingerprints of large-scale neuronal interac-

5   tions. Nat Rev Neurosci. 13(2):121–134. doi:10.1038/nrn3137.

6 Singer W. 2013. Cortical dynamics revisited. Trends Cogn Sci. 17(12):616–626.

7   doi:10.1016/j.tics.2013.09.006.

8 Singer W. 2018. Neuronal oscillations: unavoidable and useful? Eur J Neurosci. 48(7):2389–

9   2398. doi:10.1111/ejn.13796.

10 Singer W, Gray CM. 1995. Visual feature integration and the temporal correlation hypothesis.

11   Annu Rev Neurosci. 18(1):555–586.

12 Smith S, Nichols T. 2009. Threshold-free cluster enhancement: Addressing problems of

13   smoothing, threshold dependence and localisation in cluster inference. NeuroImage.

14   44(1):83–98. doi:10.1016/j.neuroimage.2008.03.061.

15 Smith SM. 2002. Fast robust automated brain extraction. Hum Brain Mapp. 17(3):143–155.

16   doi:10.1002/hbm.10062.

17 Smith SM, Fox PT, Miller KL, Glahn DC, Fox PM, Mackay CE, Filippini N, Watkins KE, Toro

18   R, Laird AR, et al. 2009. Correspondence of the brain's functional architecture during ac-

19   tivation and rest. Proc Natl Acad Sci. 106(31):13040–13045.

20   doi:10.1073/pnas.0905267106.

21 Smith SM, Jenkinson M, Johansen-Berg H, Rueckert D, Nichols TE, Mackay CE, Watkins KE,

22   Ciccarelli O, Cader MZ, Matthews PM, et al. 2006. Tract-based spatial statistics: Voxel-

23   wise analysis of multi-subject diffusion data. NeuroImage. 31(4):1487–1505.

24   doi:10.1016/j.neuroimage.2006.02.024.

1   Song S-K, Sun S-W, Ramsbottom MJ, Chang C, Russell J, Cross AH. 2002. Dysmyelination
2   revealed through MRI as increased radial (but unchanged axial) diffusion of water. Neu-
3   roImage. 17(3):1429–1436. doi:10.1006/nimg.2002.1267.

4   Song S-K, Yoshino J, Le TQ, Lin S-J, Sun S-W, Cross AH, Armstrong RC. 2005. Demye-
5   lination increases radial diffusivity in corpus callosum of mouse brain. NeuroImage.
6   26(1):132–140. doi:10.1016/j.neuroimage.2005.01.028.

7   Sormaz M, Murphy C, Wang H, Hymers M, Karapanagiotidis T, Poerio G, Margulies DS, Jef-
8   feries E, Smallwood J. 2018. Default mode network can support the level of detail in expe-
9   rience during active task states. Proc Natl Acad Sci. 115(37):9318–9323.
10   doi:10.1073/pnas.1721259115.

11   Sterr A, Müller MM, Elbert T, Rockstroh B, Pantev C, Taub E. 1998a. Perceptual Correlates of
12   Changes in Cortical Representation of Fingers in Blind Multifinger Braille Readers. J
13   Neurosci. 18(11):4417–4423. doi:10.1523/JNEUROSCI.18-11-04417.1998.

14   Sterr A, Müller MM, Elbert T, Rockstroh B, Pantev C, Taub E. 1998b. Changed perceptions in
15   Braille readers. Nature. 391(6663):134–135. doi:10.1038/34322.

16   Stevens AA, Weaver K. 2005. Auditory perceptual consolidation in early-onset blindness. Neu-
17   ropsychologia. 43(13):1901–1910. doi:10.1016/j.neuropsychologia.2005.03.007.

18   Stevens B, Porta S, Haak LL, Gallo V, Fields RD. 2002. Adenosine: A neuron-glial transmitter
19   promoting myelination in the CNS in response to action potentials. Neuron. 36:855–868.

20   Striem-Amit E, Ovadia-Caro S, Caramazza A, Margulies DS, Villringer A, Amedi A. 2015.
21   Functional connectivity of visual cortex in the blind follows retinotopic organization prin-
22   ciples. Brain. 138(6):1679–1695. doi:10.1093/brain/awv083.

23   Striem-Amit E, Wang X, Bi Y, Caramazza A. 2018. Neural representation of visual concepts
24   in people born blind. Nat Commun. 9(1):1–12.

1   Thiebaut de Schotten M, ffytche DH, Bizzi A, Dell'Acqua F, Allin M, Walshe M, Murray R,

2   Williams SC, Murphy DGM, Catani M. 2011. Atlasing location, asymmetry and inter-sub-

3   ject variability of white matter tracts in the human brain with MR diffusion tractography.

4   NeuroImage. 54(1):49–59. doi:10.1016/j.neuroimage.2010.07.055.

5   Töllner T, Wang Y, Makeig S, Müller HJ, Jung T-P, Gramann K. 2017. Two independent

6   frontal midline theta oscillations during conflict detection and adaptation in a Simon-type

7   manual reaching task. J Neurosci. 37(9):2504–2515. doi:10.1523/JNEUROSCI.1752-

8   16.2017.

9   Trouvain J. 2007. On the comprehension of extremely fast synthetic speech. Saarl Work Pap

10   Linguist. 1:5–13.

11   Tzourio-Mazoyer N, Landeau B, Papathanassiou D, Crivello F, Etard O, Delcroix N, Mazoyer

12   B, Joliot M. 2002. Automated anatomical labeling of activations in SPM using a macro-

13   scopic anatomical parcellation of the MNI MRI single-subject brain. NeuroImage.

14   15(1):273–289. doi:10.1006/nimg.2001.0978.

15   Van Ackeren MJ, Barbero FM, Mattioni S, Bottini R, Collignon O. 2018. Neuronal populations

16   in the occipital cortex of the blind synchronize to the temporal dynamics of speech. eLife.

17   7:e31640. doi:10.7554/eLife.31640.

18   Van Veen BD, Van Drongelen W, Yuchtman M, Suzuki A. 1997. Localization of brain electri-

19   cal activity via linearly constrained minimum variance spatial filtering. IEEE Trans Biomed

20   Eng. 44(9):867–880. doi:10.1109/10.623056.

21   VanRullen R. 2018. Perceptual rhythms. In: Wixted JT, editor. Stevens' handbook of experi-

22   mental psychology and cognitive neuroscience. Hoboken, NJ, USA: John Wiley & Sons,

23   Inc. p. 1–44.

1   Visser M, Lambon Ralph MA. 2011. Differential contributions of bilateral ventral anterior tem-

2   poral lobe and left anterior superior temporal gyrus to semantic processes. J Cogn Neurosci.

3   23(10):3121–3131. doi:10.1162/jocn_a_00007.

4   Voss P. 2019. Brain (re)organization following visual loss. Wiley Interdiscip Rev Cogn Sci.

5   10(1):e1468. doi:10.1002/wcs.1468.

6   Voss P, Zatorre RJ. 2012. Organization and reorganization of sensory-deprived cortex. Curr

7   Biol. 22(5):R168–R173. doi:10.1016/j.cub.2012.01.030.

8   Wake H, Ortiz FC, Woo DH, Lee PR, Angulo MC, Fields RD. 2015. Nonsynaptic junctions on

9   myelinating glia promote preferential myelination of electrically active axons. Nat Com-

10   mun. 6(1):7844. doi:10.1038/ncomms8844.

11 Wang D, Qin W, Liu Y, Zhang Y, Jiang T, Yu C. 2013. Altered white matter integrity in the

12   congenital and late blind people. Neural Plast. 2013:1–8. doi:10.1155/2013/128236.

13 Watkins KE, Shakespeare TJ, O'Donoghue MC, Alexander I, Ragge N, Cowey A, Bridge H.

14   2013. Early auditory processing in area V5/MT+ of the congenitally blind brain. J Neurosci.

15   33(46):18242–18246. doi:10.1523/JNEUROSCI.2546-13.2013.

16 Zatorre RJ, Fields RD, Johansen-Berg H. 2012. Plasticity in gray and white: Neuroimaging

17   changes   in   brain   structure   during   learning.   Nat   Neurosci.   15(4):528–536.

18   doi:10.1038/nn.3045.

19 Zhang L, Jiang W, Shu H, Zhang Y. 2019. Congenital blindness enhances perception of musical

20   rhythm more than melody in Mandarin speakers. J Acoust Soc Am. 145(5):EL354–EL359.

21   doi:10.1121/1.5100899.

22 Zhang LI, Bao S, Merzenich MM. 2001. Persistent and specific influences of early acoustic

23   environments   on   primary   auditory   cortex.   Nat   Neurosci.   4(11):1123–1130.

24   doi:10.1038/nn745.